TECHNISCHE UNIVERSITÄT WIEN

Institut für Computertechnik
Institute of Computer Technology

A MASTER THESIS ON

Impact of PV System Orientation on Grid Integration

IN PARTIAL FULFILLMENT OF THE REQUIREMENTS

FOR THE DEGREE OF

Diplom-Ingenieur

(Equivalent to Master of Science)

in

Energy Engineering and Automation Technology (UE 066 506)

by

Christopher Wappel

01643863

Supervisor(s):

Ao.Univ.Prof. Dipl.-Ing. Dr.techn. Thilo Sauter

Projektass. Dipl.-Ing. Stefan Wilker, B.Eng.

Vienna, Austria

November 2023

Abstract

Due to the rapid increase in photovoltaic installations, the power grid is increasingly reaching its capacity limits. As a result, the lack of available capacities in the distribution grid is becoming more of an obstacle and is slowing down the energy transition. The current approval process in Austria does not require that the planned or actual orientation of PV systems must be communicated to the grid operator. Therefore, it is not possible to predict the exact generation profiles in advance. Instead, currently only the threshold power is available as a basis for calculation, possibly with reduction factors. This work analyses to which extend the grid operator can enhance the integration potential of PV systems in a grid segment by knowing the orientation of all PV systems. Based on solar position data and module information, a clear sky model for a PV module was developed and implemented in MATLAB. With the help of this model one can estimate the maximum power output of a module throughout a year and use this value as a more precise basis for system sizing. A Monte Carlo simulation was conducted to investigate how the maximum installable PV capacity in a network segment increases when orientation data is available. The load flow calculations for the simulations were conducted using BIFROST in SimBench test networks. Additionally, the impact of bifacial technology modules was examined, as they are expected to play an increasingly significant role in the coming years. The work demonstrates that, depending on the used method, the knowledge of PV system orientation can increase the integration potential in a grid segment by up to 33%.

Kurzfassung

Durch den rasanten Anstieg von Photovoltaikanlagen gerät das Stromnetz immer häufiger an seine Auslastungsgrenze. Die zunehmend knappen freien Kapazitäten im Verteilnetz stellen daher ein wachsendes Hindernis dar und bremsen die Energiewende. Der derzeitige Bewilligungsprozess in Österreich sieht nicht vor, dass die geplante oder tatsächliche Ausrichtung von PV-Anlagen dem Netzbetreiber mitgeteilt werden muss. Daher kann im Voraus nicht mit den genauen Erzeugungsprofilen gerechnet werden, stattdessen steht derzeit lediglich die Engpassleistung mit ggf. Abschlagsfaktoren als Berechnungsgrundlage zur Verfügung. Diese Arbeit stellt eine Analyse dar, inwieweit der Netzbetreiber durch Kenntnis der Ausrichtung der PV-Anlagen in einem Netzabschnitt das Integrationspotenzial von PV-Anlagen erhöhen kann. Basierend auf Sonnenstandsdaten und Moduldaten wurde ein Schönwettermodell für ein PV-Modul entwickelt, welches in MATLAB implementiert wurde. Mithilfe dieses Modells lässt sich die theoretisch maximale Leistung eines Moduls im Jahresverlauf abschätzen und diesen Wert als genauere Dimensionierungsgrundlage verwenden. Unter Verwendung dieses Modells wurde anhand einer Monte-Carlo-Simulation untersucht, inwiefern sich die maximal installierbare PV-Leistung in einem Netzabschnitt erhöht, wenn Ausrichtungsdaten zur Verfügung stehen. Die Lastflussberechnung für die Simulationen wurde unter Verwendung von BIFROST in SimBench-Testnetzen durchgeführt. Zudem wurde der Einfluss von Modulen mit bifazialer Technologie untersucht, da diese in den kommenden Jahren eine immer größere Rolle spielen werden. Die Arbeit zeigt, dass das Wissen über die Ausrichtungen aller PV-Systeme, abhängig von der verwendeten Methode, das Integrationspotenzial in einem Netzsegment um bis zu 33% steigern kann.

Erklärung

Hiermit erkläre ich, dass die vorliegende Arbeit ohne unzulässige Hilfe Dritter und ohne Benutzung anderer als der angegebenen Hilfsmittel angefertigt wurde. Die aus anderen Quellen oder indirekt übernommenen Daten und Konzepte sind unter Angabe der Quelle gekennzeichnet.
Die Arbeit wurde bisher weder im In- noch im Ausland in gleicher oder in ähnlicher Form in anderen Prüfungsverfahren vorgelegt.

Copyright Statement

I, Christopher Wappel, hereby declare that this thesis is my own original work and, to the best of my knowledge and belief, it does not:

- Breach copyright or other intellectual property rights of a third party.
- Contain material previously published or written by a third party, except where this is appropriately cited through full and accurate referencing.
- Contain material which to a substantial extent has been accepted for the qualification of any other degree or diploma of a university or other institution of higher learning.
- Contain substantial portions of third party copyright material, including but not limited to charts, diagrams, graphs, photographs or maps, or in instances where it does, I have obtained permission to use such material and allow it to be made accessible worldwide via the Internet.

Signature: _____

Vienna, Austria, November 2023 Christopher Wappel

Contents

List of Tables

List of Figures

Chapter 1

Introduction

1.1 Motivation

The ongoing climate crisis and the increasing global tensions lead to an even stronger drive towards renewable and independent energy production. This trend is not only observable on state level but also on private level for houses or even cluster of houses, gaining independence with decentralized energy production- or storage systems. The primary factor in this transformation are photovoltaic systems. Especially the rapidly increased energy prices peaked in 2022 and still remaining at a high level had lead to a rush which peaked in a record in newly installed PV systems in 2022. The power of newly installed systems almost doubled over the last two years reaching to $1009\,\mathrm{MWp/year}$ for 2022 in Austria. [1] Furthermore the Austrian Government has agreed on the goal of sourcing its (national net) power supply exclusively from renewable energy sources by 2030. Therefore it can be expected that this high level of PV integration will be maintained. The target is to increase the output from new installations by $11\,\mathrm{TWh}$ until 2030, based on the 2020 levels. [2] Both material shortages and a lack of available installation staff have contributed to the challenges faced in the solar industry. Additionally, the electrical distribution grids are reaching their limits due to the surges in newly installed PV systems.

Since the expansion of power grids is not happening as quickly as needed, there is a growing number PV systems with surplus feed-in getting rejected, as well as substantial limitations of maximum feed-in power. During the installation and approval process by the distribution grid operator (DSO), currently only the nominal power output of the modules is taken into account while the orientation or other installation parameters are not considered. This implies that for the approval process, it doesn't matter whether the PV system is optimally aligned (e.g. $35°$–$40°$ south), or if it has an alignment where the nominal output can't even be nearly achieved. Consequently there may be a loss of power expansion-

potential, as systems could be built that are not optimally oriented (or from the perspective of the grid operator: not worst-case-oriented) at least to some degree. In addition, different orientations result in a variety of power generation profiles. This work aims to investigate the extent to which it is beneficial to consider the orientation when approving the installation of new PV systems.

The Grid Infrastructure Plan [3] outlines essential infrastructure requirements projected for 2030. As revealed by the Climate Ministry, it highlights a theoretical PV expansion potential of 80 $\mathrm{TWh/a}$. After consideration of economic and technical feasibility this number narrows down the realistic achievable generation potential of 10 $\mathrm{TWh/a}$. This fact underscores the importance of taking PV installation parameters into consideration.

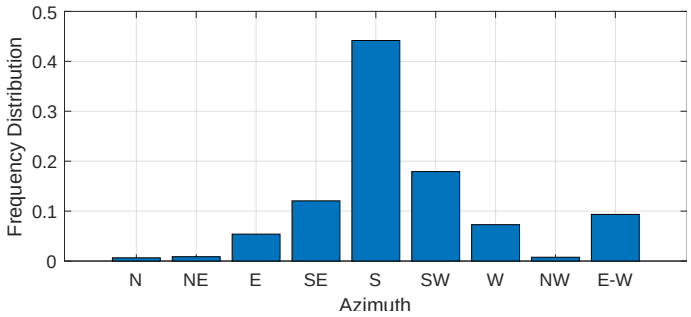

Figure 1.1: Main orientation of newly installed PV systems in Germany based on data from Jan 2020 to Apr 2022 from MaStR.

Based on the evaluation of Marktstammdatenregister (MaStR) [4] data in Fig. 1.1, approx. one third of all newly registered systems have orientations that are not directed to south (including SE and SW), which highlights the importance of alternative orientations. Existing and new systems have to be registered by the PV owners, so there is currently no evidence that DSOs use this data for any technical calculations. In Austria, there is currently no reliable comprehensive PV register available. However, there is the Anlagenregister [5] provided by E-Control, which only includes information on installed capacity, energy production from previous years and city postal codes.

1.2 Research Questions

The objective of this thesis is to evaluate whether it is necessary to consider the orientation or other installation parameters of newly installed or even for existing systems. In particular, this work will answer the following research questions:

- How big are deviations between the nominal power of photovoltaic systems according to the data sheet and the actual maximum achievable bottleneck power with special regard to the ori-

entation of the modules? Furthermore, what is the relevance of this deviation for the operation of a distribution grid?

- Is the amount of additional nominal installation power that could be unlocked in a distribution grid if the grid operator actively considers the orientation of the PV modules in a grid section substantial?

1.3 Structure of this Work

In the first step of this work, the relevant framework conditions and general calculation principles that are considered by the distribution grid operator for approving new PV installations will be examined. Specifically, the case where a grid section is almost fully utilized in terms of power and has only limited capacity available. The limiting technical parameters should be evaluated, including the thermal design of local network transformers, power lines, voltage issues with surplus feeders, and inverter bottleneck capacity.

Since this work focuses exclusively on the worst-case scenarios, no real data will be used. For this reason the PV data should be modeled using mathematical models with ideal weather data. In the next step, the power data should be simulated depending on the orientation. The simulations will be conducted using MATLAB. Conclusions will then be drawn based on these simulations. Additionally, a grid segment is modeled and simulated using BIFROST to estimate the potential for integrating PV systems.

The finalized work is intended to serve as a possible basis for decision-making for the grid operator, potentially enabling the addition of PV installations in a grid segment that would typically not receive approval. By employing extended calculations with advanced parameters, it aims to address the issue that grid expansion is currently too slow to handle all the newly installed power by PV systems.

Chapter 2

PV Approval Process in Austria

This chapter provides an overview of the state of the art grid connection approval process in 2023 of new PV systems installed in the distribution grid. First, it should be noted that in Austria there is no standardized procedure and each DSO is independently responsible for grid access. The legal basis for this is formed by the ElWOG 2010 [6] as well as the technical basis by TOR (specifically TOR C, TOR D2, and TOR Erzeuger) as outlined by the regulatory authority E-Control. The TOR defines requirements on basic parameters such as short-circuit power, voltage changes, flicker, asymmetries, harmonics, commutation dips and signal transmission interference. However, the only issues that directly limit the maximum feed-in potential are the maximum utilization of the operational assets in the grid and to stay within a given voltage threshold. Other parameters typically only impose requirements on the inverter and on other device installed in the system, but are independent of the installed PV capacity.

According to §20 ElWOG 2010, all DSOs are required to report available renewable energy capacities at grid-level 4 (substation between high-voltage (HV) 110 kV and medium-voltage (MV) 10 to 30 kV). These reports must be published on a quarterly basis. In the reference [7] fundamental calculation methods are provided for this purpose, which are described in the following points. It's important to note that just because a substation has available capacities it doesn't automatically imply approval, instead these should capture the need for network expansion. The authorization of a PV with certain power output in the low-voltage (LV) grid requires individual examination. The transparency of publicly available grid capacity information primarily aims to serve plant installers and investors in identifying potential locations for renewable power plants.

- **Precise probabilistic approach:** Requires the existence of a digital grid model. In each step power generation systems are added to grid-level 5-7 (LV and MV-grid) so that generation power and the connection point are chosen randomly. The type (PV, wind or other renewable technolo-

gies) of the generation plant is also varied randomly. This process of adding PV in each step in random batches continues until either a voltage band or a load limit violations occurs. This process can be repeated for example 1000 times leading to 1000 different integration potentials for one particular substation. This already indicates that this stochastic method does not replace individual PV testing. For instance, if one chooses the 5% quantile as the maximum integration potential. This means that in 950 out of the 1000 simulated cases a voltage band violation or thermal load violation occurred at a higher power. This would indicate that probably more PV systems can be integrated in the grid if properly located. However in 5% of the cases violations can still occur in extreme edge cases e.g., feed-in at the end of a long line.

- **Rough approach:** In this method, no simulation is conducted. Only the nominal apparent power of the transformer and measured load values from the substation are used, taking into consideration diversity factors.

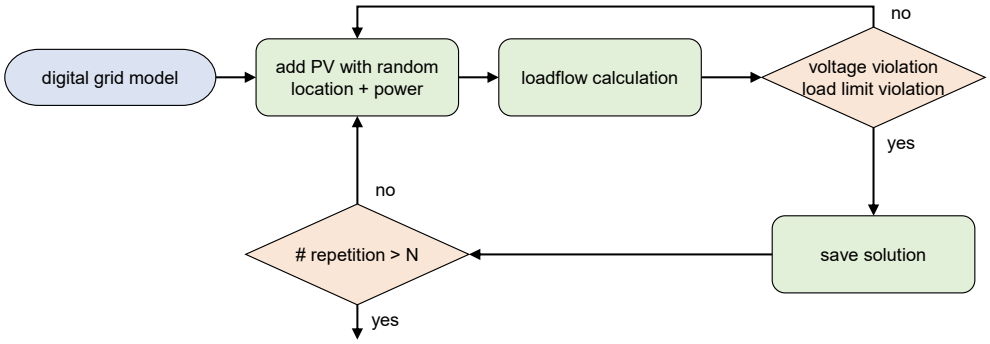

Figure 2.1: Probabilistic approach to estimate the PV capacity.

In addition to the above, two other calculation variants are proposed which represent a certain simplification of the probabilistic approach. Certain control parameters are neglected for the calculation, e.g. no On-Load Tap Changer (OLTC), no $Q(U)$-control and no time sequences are considered but rather only expected worst-case time points. The compulsory framework for calculation methods for DSOs are stated in a regulation [8] published in 2022 and its corresponding annotation with calculation examples [9].

The *available grid capacity* is defined as the sum of power from all generation plants that can be integrated to the low-voltage side of the substation. The reported *available grid capacity* is determined by subtracting the *utilized capacity* (and if applicable any *reserved capacities*) from the *maximum allowable capacity*. The *maximum allowable capacity* is usually half of the apparent power of the substation, if the substation serves end consumers. This ensures compliance with the n-1 safety requirement, which is mandatory in the HV-grid. *Utilized capacity* can be calculated by taking the maximum value (or e.g.

99.5% quantile to filter out peaks) of the measured apparent power at one substation over a year. This method thus focuses only on the worst-case days. In addition, [8] states that stochastic calculation methods are also allowed, as long as they meet the following criteria:

- $>$ 500 simulations,
- loads can be estimated,
- indicated quantile: $<$ 50% quantile
- and simulation period: year or just worst-case-day.

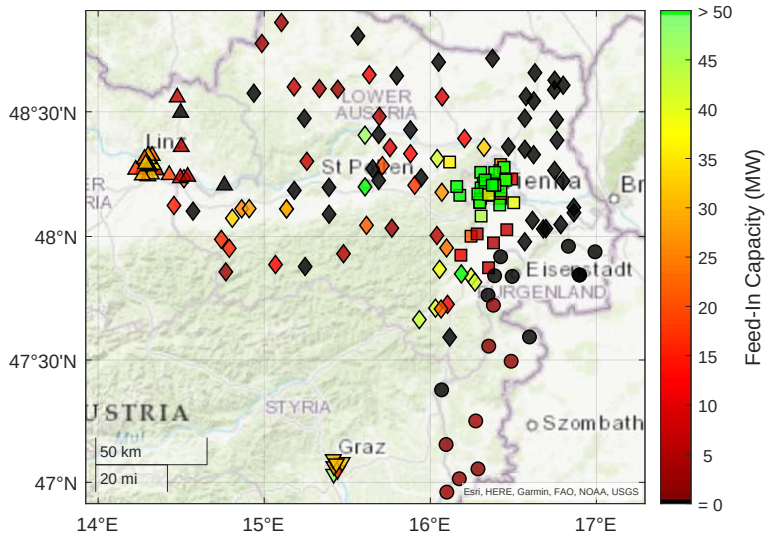

Figure 2.2: Reported available grid capacity values for following DSOs: □ Wiener Netze (date: Q4 2022), ♢ Netz Niederösterreich (date: unknown), △ Linz Netz (date: 27.4.2023), ▽ Stromnetz Graz (31.12.2022) and ○ Netz Burgenland (date: 1.4.2023). Data was taken from corresponding DSO webpages. Black markers indicate a grid capacity of 0 MV. Since Aug 2022 an overview platform has been launched, serving as a dashboard that gathers the reported capacities published by DSOs [10].

It is worth mentioning that in approximately 10% of cases, there is no available feed-in capacity due to limitations in the HV grid. Additionally, it is evident that capacity in rural areas is often fully utilized, while notably around Vienna and Graz there are still significant capacities available. In the following legal aspects are considered which are relevant for the connection process.

PVs with bottleneck power $>$ 20 kW: According to §17 ElWOG 2010, DSOs are required to assign a load profile to generation plants in their grid and report it to the balance group representative. These load profiles are generally measured with load profile meters. However, for small power generation plants connected at grid levels 6 or 7 ($\leq$ 30 kV) a standardized load profile can be used by the DSO. The use of standardized load profiles is only permissible for generators/consumers with a capacity of $<$ 50 kW and an annual production of $<$ 100 MWh. Standardized load profiles are published for different plant technologies. The profile for PV systems, which can be seen in Fig. 2.3 is not continuous

over a year but is split into seasons and need to be adapted to the system's peak power by the DSO. However these load profiles are only used for subsequent technical clearance and to coordinate deviations with balancing energy demand. Thus it is not assumed that DSOs use these load profiles as a basis for the approval process. For large-scale plant operators its known that they request the system orientation in order to make estimates for the schedules. To get approval a grid connection fee has to be paid to the DSO which compensates all the costs associated with grid connection. It is a tiered flat rate per kW-peak unless the connection cost exceeds $175\,€/\mathrm{kWh}$. In this case the customer has to pay the excess amount.

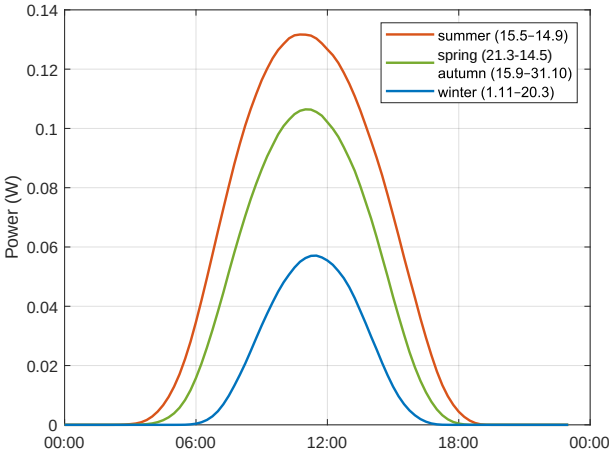

Figure 2.3: VDEW standard load profiles for feed-in PVs as stated in [11], defined according to seasons. Each profile represents the average value within a 15-minute interval. The curves are normalized to an annual yield of $1000\,\mathrm{kWh}$ and need to be adjusted to fit the real system. Although not explicitly specified, the curve would correspond to an orientation of approx. $0/25$ to $0/30$.

PVs with bottleneck power $\leq$ 20 kW: Power plants based on renewable energies can be connected using a simplified approval process based on §17a ElWOG 2010. After reporting the plant to the DSO, the DSO has to grant feed-in permission withing four weeks unless there are well-founded safety concerns regarding the grid. Additional granted PV systems have the right to 100% surplus feed-in without limitation. The grid connection fee is the same as for systems with $> 20\,\mathrm{kW}$ systems with the benefit that in the case of an existing grid connection point (for consumption), the fee is reduced because the payable connection load can be decreased by the nominal already connected demand load. [12]

The subsequent two chapters will discuss the technical background behind the two restrictive factors related to the available integration potential.

2.1 Thermal Utilization Limits

The compliance with the maximum ratings of all network components can be checked in advance through a simple load flow calculation. For this purpose the existence of an existing digital network model is favorable, although for low voltage level it is often only available for larger DSOs.

If power measurement values are available, for example at the terminals of the distribution transformer the calculated bottleneck power can be compared with the actual real values. Based on the guidelines for calculating the available power capacities at a substation specified in KBM-VO [9], the measurements can be clustered over the entire observation period (should be > 1 year), e.g. using 5-minute averages. To exclude one-time special effects the 99.5% quantile is selected as the maximum load flow value. This maximum value can then be compared with the result of the load flow calculation to check for plausibility.

2.2 Voltage Band Violations

According to §8 END-VO 2012 [13], DSOs are required to ensure that the voltage at each grid connection point conforms to the parameters specified in EN 50160, with specific emphasis on ensuring that the voltage is within a $\pm 10\%$ range of the nominal voltage. Feed-in at the connection point leads to a voltage increase throughout the entire network due to the reversed the power flow. When calculating the amount of the voltage increase, it is helpful to consider the short-circuit power of the higher-level network. The short-circuit power

$$S_k = \frac{c\, U_n^2}{Z_k} \tag{2.1}$$

is the power that arises when nominal voltage is present at the short-circuit location and the short-circuit current is limited only by the short-circuit impedance Z_k. Factor c accounts for possible voltage deviations withing the $\pm 10\%$ range. Since short circuits do not occur at full nominal voltage, S_k is just a theoretical value, but it is useful for characterizing the network impedance. For maximum feed-in power calculation, the smallest possible short-circuit power (highest Z_k) must be considered.

Basic principles for calculating the voltage rise and the assessment of other network disturbances can be found in TOR D2 [14]. The relative voltage increase at an arbitrary location x in the network can be determined using the short-circuit power $S_{k,\mathrm{x}}$ and network angle $\varphi_{k,\mathrm{x}}$ at location x with the approximation

$$\Delta u_\mathrm{x} = \frac{U_n - U_\mathrm{x}}{U_n} \approx \frac{S_\mathrm{PV}}{S_{k,\mathrm{x}}} \cos(\varphi_{k,\mathrm{x}} - \varphi_\mathrm{PV}). \tag{2.2}$$

A detailed mathematical derivation can be found in the lecture recording of Jörn Loviscach [15]. φ_{PV} in this context represents the phase angle of the feed-in power by the inverter, typically $< \arccos(0.9) = 45°$. Further details are described in the following subsection. When multiple PV systems are feeding in, voltage rise needs to be superposed. From (2.2) it follows that the voltage increase depends on fixed parameters (line impedance, line length) represented in Z_k, as well as S_{PV} with corresponding angle φ_{PV}. Therefore feed-in power is the only limiting parameter of the system.

Effect of Reactive Power Injection

In the following the relationship of reactive feed-in power and the voltage is briefly derived. Assuming that the feeder where the PV system is connected has a complex impedance of $\underline{Z} = R + \mathrm{j}X$. Thus the voltage drop along the feeder results in

$$\Delta\underline{U} = \underline{U}_L - \underline{U}_{\mathrm{PV}} = \underline{Z}\,\underline{I}. \tag{2.3}$$

$\underline{S}_{\mathrm{PV}}$ represents the apparent power generated by the PV inverter at the end of the feeder, while $\underline{S}_L$ represents the load consumption at the other end. $\underline{U}_{\mathrm{PV}}$ and $\underline{U}_L$ are the corresponding complex voltages at both ends of the line. The branch current flowing in the feeder is calculated based on the voltage and apparent power at both nodes

$$\underline{S} = \underline{U}\,\underline{I}^* \quad \Longrightarrow \quad \underline{I} = \frac{\underline{S}^*_{\mathrm{PV}}}{\underline{U}^*_{\mathrm{PV}}} = \frac{\underline{S}^*_L}{\underline{U}^*_L}. \tag{2.4}$$

Substituting the current for the PV connection point leads to

$$\Delta\underline{U} = \underline{Z}\,\frac{\underline{S}^*_{\mathrm{PV}}}{\underline{U}^*_{\mathrm{PV}}}, \tag{2.5}$$

$$U_L \mathrm{e}^{\mathrm{j}\delta_L} - U_{\mathrm{PV}}\mathrm{e}^{\mathrm{j}\delta_{\mathrm{PV}}} = \frac{(R+\mathrm{j}X)(P_2 - \mathrm{j}Q_2)}{U_{\mathrm{PV}}\mathrm{e}^{-\mathrm{j}\delta_{\mathrm{PV}}}}. \tag{2.6}$$

Assuming a small angle deviation ($\delta_L \approx \delta_{\mathrm{PV}}$), the angular terms cancel out in (2.6), resulting in the approximation

$$U_L - U_{\mathrm{PV}} \approx \frac{(R+\mathrm{j}X)(P_{\mathrm{PV}} - \mathrm{j}Q_{\mathrm{PV}})}{U_{\mathrm{PV}}} = \frac{RP_{\mathrm{PV}} + XQ_{\mathrm{PV}} + \mathrm{j}(XP_{\mathrm{PV}} - RQ_{\mathrm{PV}})}{U_{\mathrm{PV}}} \tag{2.7}$$

for the voltage drop. Splitting the equation into its real component yields the following approximation equation

$$\Delta U \approx \frac{RP_{\mathrm{PV}} + XQ_{\mathrm{PV}}}{U_{\mathrm{PV}}}. \tag{2.8}$$

In (2.8) it can be observed that as demonstrated at the beginning of the chapter a active power injection $P_{\mathrm{PV}} > 0$ leads to a voltage rise. Furthermore it is evident that a reactive power injection $Q_{\mathrm{PV}} < 0$ can actively counteract this voltage rise.

2.2.1 $Q(U)$-control

In order to maintain high voltage quality, PV inverters have to comply with requirements regarding $Q(U)$-control, which are specified in [16] and can be prescribed by the DSO. Inverters must be capable of providing a power factor of $\cos\varphi = 0.9$ both inductive and capacitive. Therefore, the reactive power supplied by the inverter is within the range of $\pm\sqrt{1-0.9^2} \approx \pm 31.2\%$ of the nominal apparent power. In the case of inverters with an apparent power of $S \leq 3.68\,\mathrm{kVA}$ a power factor of $\cos\varphi = 0.95$ is sufficient. Providing reactive power by the inverter compensates for inductive reactive power from the grid, which leads to a reduced load flow and results in an increased voltage. Subsequently inverters have to provide inductive reactive power to increase voltage as shown in Fig. 2.4(a). If the voltage increase is still not sufficient, the maximum produced power has to be gradually reduced before completely shutting down feed-in due to overvoltage, shown in Fig. 2.4(b).

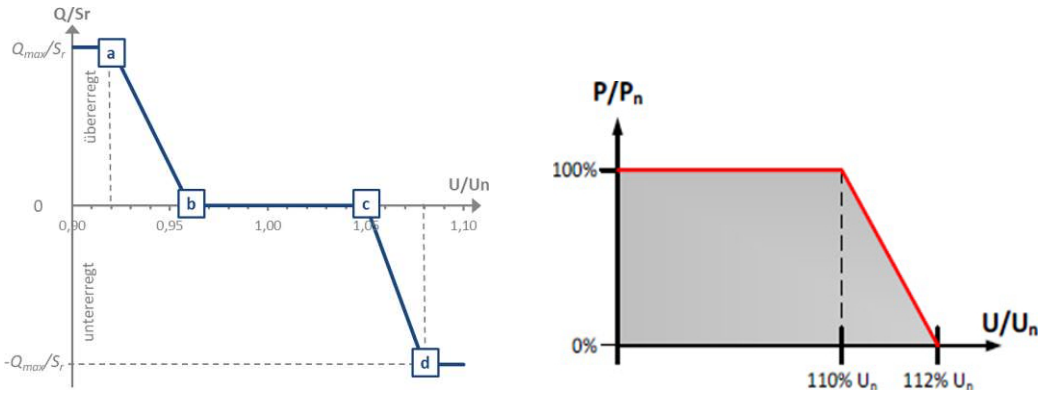

(a) $Q(U)$-control (b) $P(U)$-control

Figure 2.4: Characteristic curves adjusting the active and reactive power generated by an inverter, aiming to control the voltage at the grid connection point. Graphs taken from [16]. The parameters in (a) need to be provided by the DSO, while standard values can be referenced from the appendix of [16].

In rural areas with overhead power lines covering longer distances and overall higher line impedance, the effect of $Q(U)$-control is higher.

2.2.2 On-Load Tap Changer

Although more commonly used in HV-MV transformer levels, another method for actively influence voltage variation is through the use of OLTCs. The voltage is adjusted by changing the number of windings used on the secondary side, for example if the measured voltage at a particular node falls

outside the acceptable range of 5%. [17] However a drawbacks is that the distribution network has to be equipped with a step transformer, as well as corresponding sensors placed throughout the distribution grid. Additionally, implementing OLTC requires more control effort, and compared to the $Q(U)$-control, this centralized method is more susceptible to critical system errors.

2.3 Individual PV Approval by DSO

The individual approval is the responsibility of each DSO, taking into account its own grid topology, such as radial and ring networks as well as performing load flow calculations. The regulatory framework developed by E-Control and DSOs specifies the requirements for power generators as outlined in TOR Generators Typ A [16], which are obligatory. It generally applies to all power generation systems $< 250\,\mathrm{kW}$. For other power generation plants with higher capacity stricter requirements are specified in further documents. However these requirements are not considered as relevant for PV systems, as this thesis focuses on the integration of smaller sized distributed power generation.

Assessment is also made regarding TOR Part D2. The DSO prepares a connection concept including parameters such as P_{max}, reactive power provision, etc. If full feed-in is not technically possible, measures such as limited feed-in power, voltage regulation, and increased short-circuit power can be prescribed.

2.3.1 Concept of Grid-Related Power

As of the summer 2023 the regulatory framework intends that the DSO treats consumption and generation separately. This means that the agreed-upon connection power is defined based on either the maximum feed-in power or the maximum consumption power. The defined maximum power P_{max} at the grid connection point for feed-in refers to either the bottleneck power of the inverter or the sum of the nominal power of all PV modules or the max. consumption power. In order to provide more flexibility to the DSO as well as to the consumer/producer, the concept of grid-related maximum is proposed in [18]. In order to provide more flexibility to DSO but also to the consumer/producer the concept of *grid-related power* is proposed in [18]. The term *grid-related power* refers to the maximum power of the entire system that can become effective at the grid connection point. The same concept could also be applied in connection with various variable generators (e.g., 2 PV systems with different orientations), with the difficulty that they are not connected at the same point but rather distributed in the grid. Moreover, this can also be observed in the context of battery systems, where more complex control algorithms can limit the power at the grid connection point. However, according to the official binding regulation only the P_{max} is decisive yet.

Chapter 3

Data Acquisition and Verification

This section aims to elaborate a model of a PV system that outputs the power curve of a PV system based on the given orientation (azimuth and tilt angle). The convention used for defining the azimuth angle is as follows: $90°$ for west, $0°$ for south, $-90°$ for east and $\pm 180°$ for north. While this convention is not standardized, it is commonly used in the field of PV systems. A slope of $0°$ indicates that the module is parallel to the earth's surface, while a slope of $90°$ means that the module is oriented perpendicular to the earth's surface. In further work, the writing convention Azimuth α_M / Slope θ_M is used to describe the fixed orientation of a PV cell in space, not to confuse this with the changing azimuth and elevation angles of the sun α_S/θ_S. To eliminate time shift, the time is represented in UTC. If the location is not specified otherwise, the coordinates of Vienna (latitude 48.2, longitude 16.4) are used.

DSOs consider the bottleneck power as the limiting factor, which can be either the nominal power of the inverter or the sum of the nominal peak power ratings of all installed modules. Since inverters have the best efficiency when operating close to their nominal power, PV systems are usually overloaded. This means that the nominal power of all modules is larger than the nominal power of the inverter. Due to this, a small power loss may be accepted depending on the installed orientation when solar irradiation is high because power peaks are then clipped by the inverter. Therefore, the nominal power of the inverter can always be considered as a lower limit. Section 4.3 shows how actively using the feed-in limitation setting of the inverter impacts the power grid. The great advantage of PV, in contrast to e.g. wind, is that one can predict the exact power curve when knowing the orientation since wind is not as predictable. This fact should be utilized in the following.

The power grid is not considered in the first place, only the effect of orientation on maximum power

should be taken into account primarily. Since the grid must be sized for the worst-case scenario, which means that the PV system is operated under optimal conditions. Therefore, the model calculates the optimal power output based on global radiation data using a clear sky model, without considering any weather effects.

3.1 Clear Sky Model

Although there are several PV simulation tools available, their main focus is on simulating with historic weather data. Foremost among them is PVGIS [19], which was later partially used for validating the PV model. In the following, specific algorithms which are partly implemented in the MATLAB PV_LIB Toolbox [20] are used. PV_LIB contains a collection of standard functions and algorithms for solar models and power systems that are useful for PV calculations. The toolbox was initially developed by Sandia National Laboratories, USA.

In the first step the sun path is calculated using the solar positioning algorithm (SPA) for a specific location over the period of one year. This algorithm delivers the azimuth and elevation angles (complementary to zenith angle) of the sun over time. In the next step, the global horizontal irradiance GHI in $\mathrm{W/m^2}$ is derived using the Haurwitz clear sky model, which only depends on the zenith angle. Comparing with real-world data, the Haurwitz clear sky model showed an overall better result over the period of one year than other available models like Ineichen-Perez. In order to calculate the irradiation data on tilted planes, which is later used for the PV simulator, the total horizontal irradiance

$$GHI = DHI + DNI \sin(\theta_S) + RHI \tag{3.1}$$

can be split up into three components: A direct component DNI (Direct Normal Irradiance) which represents the portion of solar beam radiation that directly reaches the surface without being affected by the atmosphere, a diffuse component DHI (Diffuse Horizontal Irradiance) which is the part of light that is scattered by earth's atmosphere and RHI (Reflective Horizontal Irradiance) which represents the reflected horizontal irradiance. This albedo component is neglected since its impact is relatively small and largely depends on the environment, making it difficult to precalculate for a general environment.

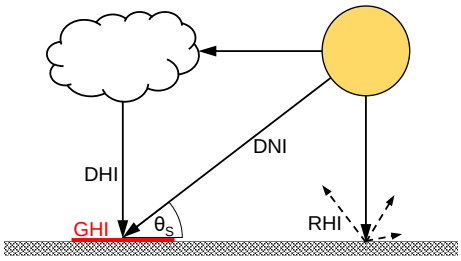

Figure 3.1: Global irradiation components.

So far, only the total radiation for a module parallel to earth was calculated. To retrieve the GTI (Global Tilted Irradiance), the angle between the plane's normal vector and the vector directly pointing from the sun to the module has to be considered. The angle of incidence γ can be simply calculated by using both the module orientation α_M/θ_M and the sun position α_S and elevation θ_S to

$$\gamma = \arccos\big(\cos(\theta_M)\sin(\theta_S) + \sin(\theta_M)\cos(\theta_S)\cos(\alpha_M - \alpha_S)\big) \tag{3.2}$$

according to [21]. With γ, the direct component for a tilted surface can simply be derived by projecting DNI onto the plane

$$DNI_{tilt} = DNIcos(\gamma). \tag{3.3}$$

However, since the diffuse component comes from all directions, a sky model has to be used as described in [22], which takes into account this anisotropic behaviour by calculating the sky view factor

$$SVF = \frac{1}{2}\big(1 + cos(\theta_M)\big) \tag{3.4}$$

which represents the portion of the sky visible to the module. For example, if it is oriented perpendicular to the earth's surface the effective sky area is reduced because only half of the irradiance can be received from the sun resulting in an $SVF = 0.5$. Thus, in general diffuse irradiance is maximized for horizontally oriented modules. For this work, the Perez Diffuse Radiation Model (parameter set of 1990) was used to determine DHI_{tilt}, which involves solving nonlinear equations implemented in the PV_LIB Toolbox. Although computationally more expensive, the Perez model showed the best fit to real-world data. The total irradiance on the tilted module can then be calculated by summing up the two projected components: $GTI = DNI_{tilt} + DHI_{tilt}$. Fig. 3.2(a) shows the calculated result over one day.

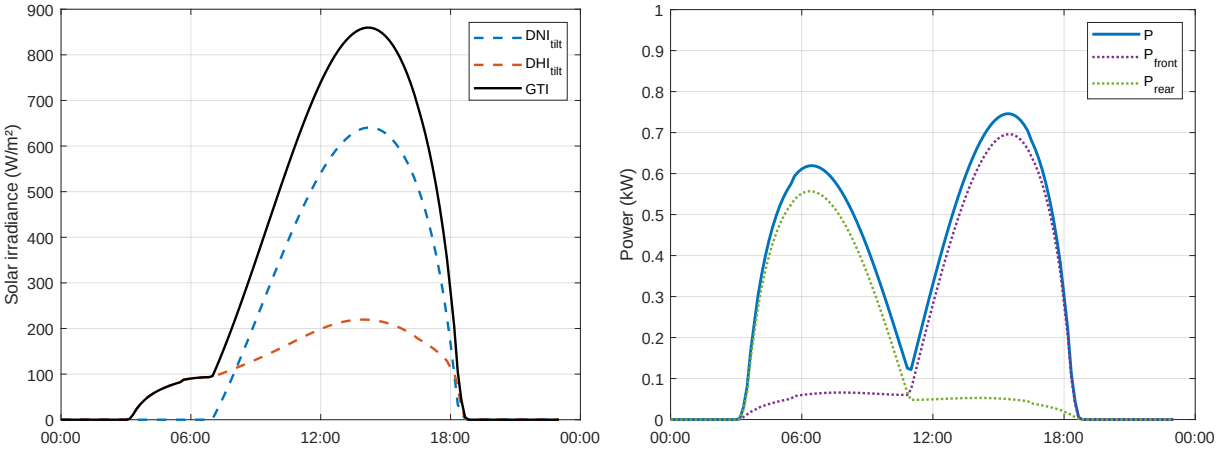

(a) Calculated direct and diffuse radiation components of global radiation on a tilted plane with a $120/40$ orientation on 21 Jun.

(b) Simulated power output of a bifacial module with a $90/90$ (vertical east-west) orientation. Difference in peak height is due to bifaciality factor, further results are discussed in section 3.5.

Figure 3.2: Simulation results for monofacial global irradiance and bifacial power on 21 Jun.

Overall, diffuse radiation accounts for approximately 30% of the total radiation measured by yearly energy production. This share varies only slightly with changing orientation. As observed in Fig. 3.2(a), diffuse radiation becomes particularly significant for orientations facing north and tilt angles greater than $20°$, as the direct radiation component is smaller for these orientations. A quick check shows that the peak around $850\,\mathrm{W/m^2}$ (depending on the day, location, and orientations) aligns well with the solar constant, which is defined to be $1367\,\mathrm{W/m^2}$.

3.2 PV Model

Using a simple PV model, radiation data is converted into power which represents the inverter output power of a PV system. The peak power of each simulated system is standardized at $1\,\mathrm{kWp}$. The aerial nominal power density (of a module) was evaluated using a sample from the module database [23], based on the years 2022 and 2023. It was calculated to be approx. $S_M = 4.8\,\mathrm{m^2/kWp}$. The efficiency parameter for a module was chosen to a typical value of $\eta_M = 0.2$, while the efficiency of the inverters was approximated as $\eta_I = 0.95$ neglecting the influence from current output power for simplicity reasons. Therefore, the PV power is calculated as

$$P = GTI\ \eta_M\ \eta_I\ \frac{S_M}{1kWp}. \tag{3.5}$$

3.2.1 Influence of Temperature

The calculated values above are valid under Standard Test Conditions (STC) with a nominal cell temperature of 25 °C. To determine the ambient temperature values, typical meteorological year (TMY) data generated by PVGIS was used, which incorporates satellite observations from 2005 to 2019 on an hourly basis. To smooth the data and eliminate short-term fluctuations, a 20-day mean filter was applied. A 20-day filter was found to be suitable since a longer filter period would eliminate daily extremes too much, while for a shorter one daily fluctuations would still be present. It is important to note that there are more precise methods and longer time periods available for this purpose. However, the selected approach is considered sufficient for the scope of this work. A typical temperature coefficient as stated in a datasheet of $-0.35\,\%/\mathrm{K}$ was used. Since the maximum possible power for grid integration is relevant,

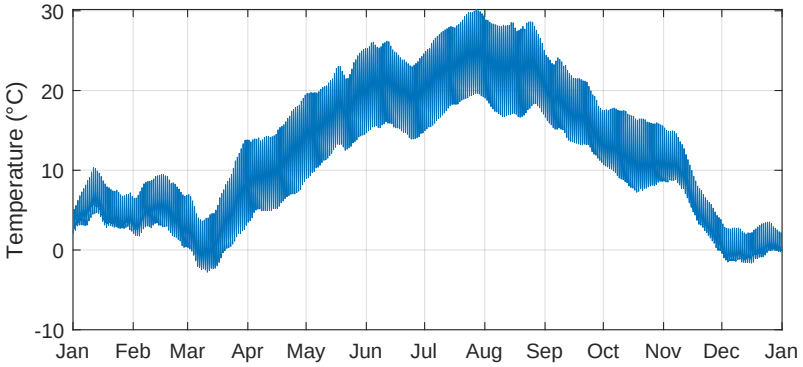

Figure 3.3: Hourly TMY data used for simulation.

the minimum possible temperature for every location should be considered. Although temperature data is available for arbitrary locations, the exact module temperature can vary significantly due to local factors such as building shading and wind patterns, which are not accurately represented in the provided data. However, these factors were generally taken into consideration during the fine-tuning of efficiency parameters by overestimating the power.

3.3 Verification

Verifications were mainly conducted using two existing systems and the real value simulation taken from PVGIS. Both real systems use a Fronius inverter, which allows the generated power to be exported at a 5-minute resolution. However the operation period of both systems was constrained to a single year. In this step the fine tuning of PV efficiency parameters has been done to ensure that the simulated PV curves closely match the actual system's performance for almost all time points.

First, comparing with an east-west system ($55/10$ and $-125/10$) installed on a flat roof in Perchtolds-

dorf, as shown in Fig. 3.4. The inverter has a nominal normalized power of $0.83\,\mathrm{kWp}$, therefore it is not possible to have a larger power output value. The data from PVGIS fits very well with the introduced clear sky simulation model. The overall power values are smaller, mainly because PVGIS uses a default system loss of 14% (for inverter and all components) which is considered to be too high. The model considers only a 5% loss, which explains the approx. 10% deviation. When comparing with the real system, on some days a power peak can be found where the output power exceeds the simulated value, although generally fitting very well. This only appears to happen on cloudy days. Considering real temperature values on these specific times points, no temperature abnormality could be found. There is no explanation, but since these peaks do not appear on clear sky days and not in summer (where the power peak value is crucial), the model could still be a good approach for estimating the power peaks over a year.

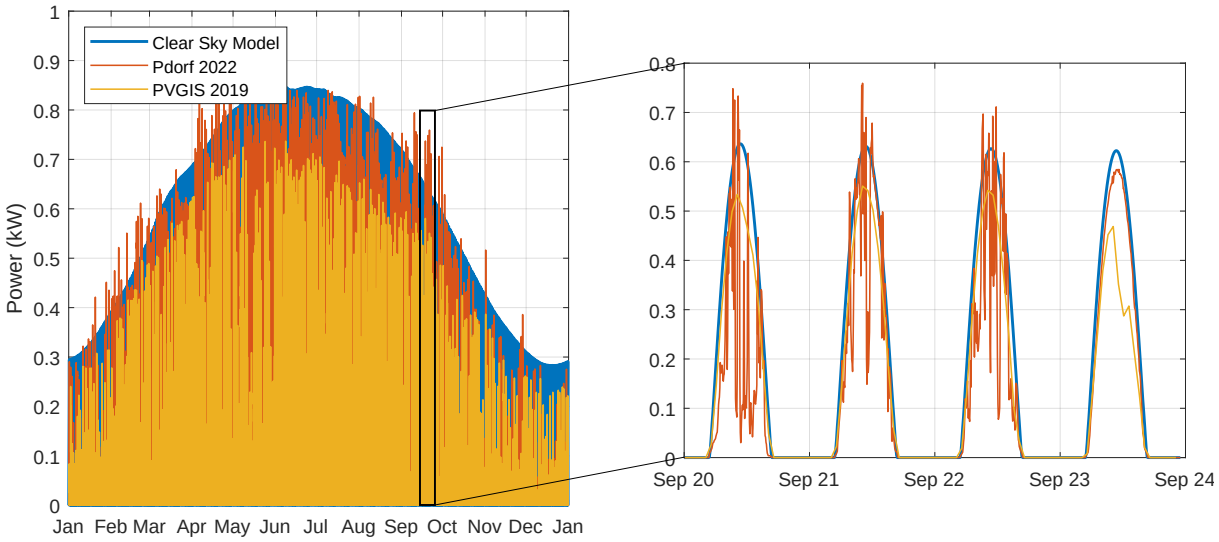

Figure 3.4: Comparison of the introduced PV simulator with an existing simulation and system for $55/10$ and $-125/10$ orientation. The right picture provides a zoomed-in view where the real system, where unfortunately despite impacted by weather conditions, the real system surpasses the clear sky model for some distinct time points.

The second system used for verification is located in Neustift and der Lafnitz, oriented with a $60/40$ and $-120/40$ configuration and mounted on a slanted roof. It has a normalized nominal inverter power of $0.9\,\mathrm{kWp}$. As a whole year of data is not available, power data from 2023 was used to fill in the missing data. Data from Jan to Apr is from 2023, while data from May to Dec represents power values from 2022. Unfortunately now even more peaks observed in Fig. 3.5 especially during the summer, where the maximum value is even more crucial. However, as described above these peaks tend to occur only on

bad weather days where power curve is not smooth. Compared to the real weather, no trend could be found that these peaks even appear on exceptionally cold days. For further investigation, an additional safety factor may be useful. However, over a larger number of systems these peaks may average out as weather conditions can vary slightly. Since the model fits very well with PVGIS, and even better for the first example, no parameters were changed.

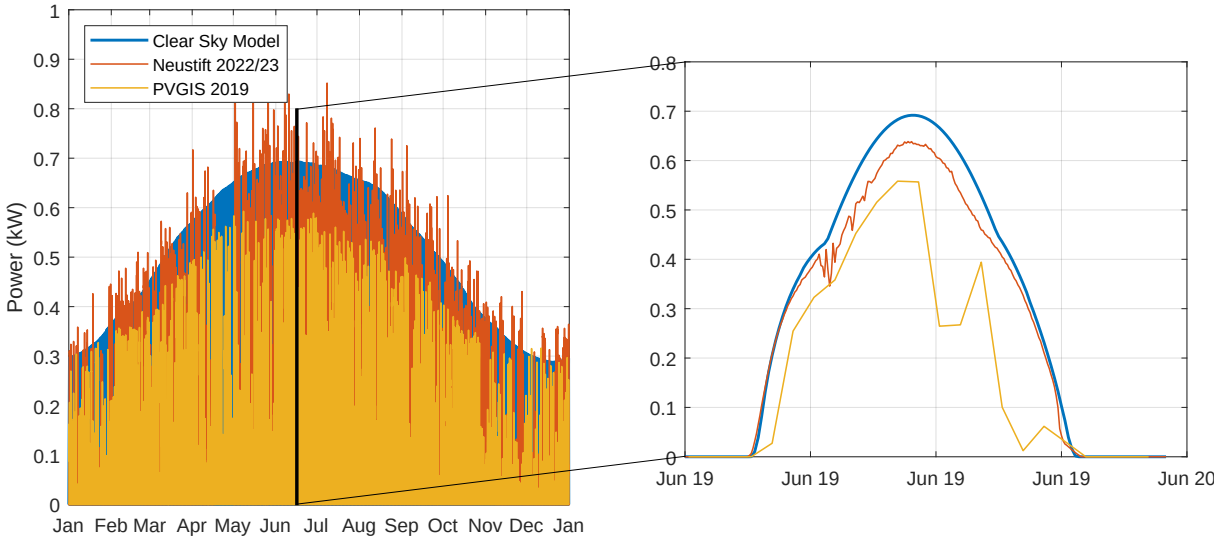

Figure 3.5: Simulation verification on a $60/40$ and $-120/40$ system. In the excerpt on the right, one can see that on a day with favorable clear weather conditions in 2022 the effect of diffuse radiation is accurately reflected in the real system.

3.4 Clear Sky Yield

For further investigations in this work sometimes the clear sky yield is used. Comparing the ideal yearly yield with the real weather yield for a specific location and orientations can provide valuable insights. This may show if the weather affects all orientations equally or has a special impact on, for example south orientation. In literature the clearness index k_T is usually used which is defined as

$$k_T = \frac{GHI_{\text{meas}}}{GHI_{\text{extra}}}, \tag{3.6}$$

which is the ratio between measured irradiation data and the calculated extraterrestrial radiation unaffected by the atmosphere [24]. The defined factor k_T is a measure in the range of $[0, 1]$, indicating the level of optimal weather conditions at specific time points. Daily average values are also available, primarily dependent on the location, however these values are only defined for horizontal plane radiation

and specific time points. In the context of this work where a rough overall estimation of the weather conditions is sufficient, k_T values are not used. By running simulations with multiple samples using various orientations and locations, the ratio between the annual yield under real weather conditions and the clear sky yield could be identified to be approx. between 60 and 70%. A time horizon of 5 years was investigated here. It primarily depends on the azimuth angle and remains relatively constant at around 60% for a south orientation. Real weather yield was taken from PVGIS simulation. As a rule of thumb, 1000 full load hours are typically assumed for a PV system in these latitudes. For the simulated PV system under clear sky conditions, this mounts to approx. 2000 full load hours, representing the theoretical upper limit of energy production. In the case of a $1\,\mathrm{kWp}$ system with an orientation of $0/30$, this leads to $2090\,\mathrm{kWh}$ or 2090 full load hours respectively.

3.5 Bifacial Module Model

Especially in recent years solar cells with bifacial technology have been gaining increasing popularity and it is even expected that they will dominate the market in the next couple of years. In comparison to monofacial modules, bifacial modules have a glass cover on the back instead of a white sheet. Rear side contacts are designed to allow sunlight to pass through, enabling them to generate power on the rear side as well. Basically, there are two system approaches for bifacial systems: First, one can simply improve efficiency for flat-angle systems by using bifacial modules. On the other hand, it enables the vertical installation of modules allowing their use in new applications such as for fences, as facade integration or in agriculture. For small tilt angles, the additional energy gain mainly results of receiving more indirect radiation. However, for larger slopes modules can also receive direct irradiance on the rear side. This fact is primarily used in the emerging field of agricultural PV systems, where bifacial PV modules are often vertically aligned, while still allowing the usage of the soil in-between for farming. [25] On average the increase in yield compared to monofacial modules is about 15 to 25%, depending on orientation. However, the major advantage lies much more in the grid-friendly generation profile.

The bifaciality factor is defined as the ratio

$$\varphi = \frac{\eta_{\mathrm{rear}}}{\eta_{\mathrm{front}}} \tag{3.7}$$

of efficiencies for both sides, which are measured independently at STC while the opposite side is covered with a non-reflective sheet, respectively. In the literature, there exist various other definitions for

calculating φ, such as the ratio of open circuit voltages or the ratio of short circuit currents. [26] Typical values vary based on cell architecture but are all within the range of 70 to 100%. For further calculations $\varphi = 75\%$ is used since this is a common value for PERC-type (Passivated Emitter and Rear Cell) cells, which currently hold a dominant position in the bifacial market. For the purpose of simplification, it is assumed that the module is infinitely thin. Therefore the point where direct radiation changes its direction towards the front module side at approx. 11:00, it shows a sharp peak in Fig. 3.2(b), whereas in reality this would be a smooth transition due to the thickness of the module.

Regrettably there are inconsistent labelings for rated peak power for bifacial modules. TÜV Rheinland proposed, as specified in IEC TS 60904-1-2 [27] the BSTC (Bifacial STC) which defines the following test conditions: G_{front} = $1000\,\mathrm{W/m^2}$, G_{rear} = $135\,\mathrm{W/m^2}$, AM = 1.5 and Cell Temp. = $25\,^{\circ}\mathrm{C}$. The backside irradiation value of $135\,\mathrm{W/m^2}$ was probably chosen since this is a typical value for an average albedo parameter α = 0.2 ($G_{\text{rear}} \approx \alpha\, \varphi\, G_{\text{front}}$). For the BSTC test case, the total effective irradiation of a module then results in

$$G = G_{\text{front}} + \varphi\, G_{\text{rear}} = 1000\,\mathrm{W/m^2} + \varphi\, 135\,\mathrm{W/m^2}. \tag{3.8}$$

However, there is still a lack of usage from manufacturers of BSTC ratings. In addition the actually achievable maximal power depends largely on the real environment in which the module is installed, since BSTC only deals with an average assumption. Some manufacturers use alternative rear side irradiation specifications for deriving the nominal power rating for their modules, such as at $300\,\mathrm{W/m^2}$. In the following, for this work therefore only the STC rating of the front side P_{front} is used to define a module. Consequently, the nominal rear side rating is $\varphi\, P_{\text{front}}$.

Typically power ratings of modules are declared and reported to the DSO using only the front side nominal power at STC. However, it's important to consider that bifacial modules have the potential to generate even higher power outputs, which will be important for DSOs in future if more bifacial modules are installed in the grid. For instance a 370 W (STC) module has a BSTC rating of 414 W. [28]

As already indicated, in contrast to monofacial modules the reflective component RHI (reflective horizontal irradiance) plays an important role for bifacial modules. The albedo coefficient α defines here the relative amount of reflected irradiance. The albedo factor is usually 0.2 to 0.3 for normal surfaces. But it must be taken into account that it can quickly change even for an existing environment. For example fresh snow can increase albedo to 0.8, which however is not that critical since the bottleneck

for feed-in capacity is typically in summer. Usually the albedo factor tends to decrease over time due to contamination and roughening of surfaces.

Table 3.1: Typical albedo coefficients for different surface materials according to [29].

Surface	α	**Surface**	α
Corrugated roof	0.1 - 0.15	Trees	0.15 - 0.18
Red/brown roof tiles	0.1 - 0.35	Oceans	0.05 - 0.1
Brick/stone	0.2 - 0.4	Grass	0.25 - 0.3
Asphalt	0.05 - 0.2	Fresh snow	0.81 - 0.88
Concrete	0.25 - 0.7	Old snow	0.65 - 0.81
White paint	0.5 - 0.9	Ice	0.3 - 0.5
Coloured paint	0.15 - 0.35		

Currently the grid is primarily south-oriented and the introduction of bifacial modules could help to enable additional capacities. Therefore in the grid simulation in section 5.5.1 bifacial modules will be addressed separately. For simplicity reasons the albedo coefficient was assumed to be constant with $\alpha = 0.25$ for all systems.

Chapter 4

PV Simulation and Analysis

In this chapter, the maximum power value for each orientation should be evaluated, which could be considered as a crucial design parameter for the grid by the DSO in the future. Considering multiple systems, it is also important to know when these power peaks occur since one cannot simply add the power peaks of individual systems when they are at different time points, varying both on a daily and hourly basis. Taking the simple example of two systems in Fig. 4.1 one can see that even for the worst case, peaking at $0.88\,\mathrm{kW}$, the PV systems cannot reach their nominal power. By examining the time profiles, one might come up with the idea that by individually limiting the inverter feed-in power, the PV operator can already account for the maximum possible power for his specific orientation. This would make the question of orientation by the DSO obsolete. But, adding up these individual peaks (could be set as threshold for feed-in limitation power of the inverters) leads to $1.76\,\mathrm{kW}$, which is however still an overestimation because the real maximum possible power value of both systems is $1.51\,\mathrm{kW}$ for the worst possible day. Comparing it with the nominal power of $2\,\mathrm{kW}$ for the whole system, which the DSO needs to account for given the unknown orientation, it shows that in this case approximately 32% could be additionally installed to conform with the $2\,\mathrm{kW}$ threshold and 16% if feed-in limitation was set to the edge of max. achievable power of one system.

Because some formulations may be highly specialized and not easily available in explicit mathematical equations, a simulation approach was conducted rather than solving for an analytic solution. The angle resolution for both the azimuth and slope angles was chosen to be 300 points, resulting in 300^2 test systems. Thus the angular resolution for the slope is $0.3°$ and $1.2°$ for the azimuth angle.

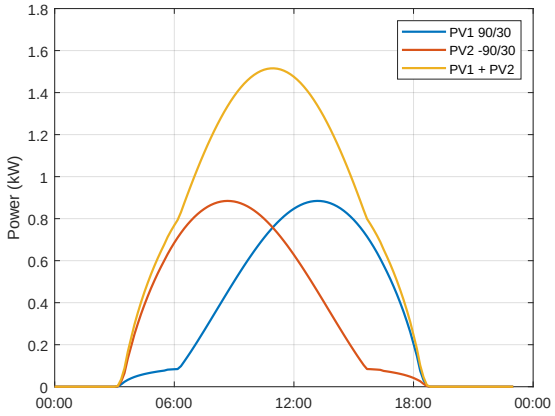

Figure 4.1: Example of an east-west system considering its maximum power values for 21 Jun.

4.1 Power Peak Analysis for a Single PV System

The power data for each system was analysed for the scope of one year. The respective points at which the maximum power value occurs are recorded, including their value and timestamp. The result of the simulation is shown in Fig. 4.2 for the maximum value and in for the corresponding time points in Fig. 4.4. As can be seen, the maximum achievable power output for any possible system orientation is $0.94\,\mathrm{kW}$, which happens to be for the $0/25.2$ orientation. This fact indicates that in any cases regardless of the orientation, either the threshold power of the system or the inverter's nominal power can be chosen at 95% of the module power. Unfortunately, the curve has a relatively flat curvature around its maximum point, which means that for most flat tilt angles with southerly direction the maximum power can still exceed $0.8\,\mathrm{kW}$. For other directions however, the maximum achievable power quickly decreases, though for these orientations there is a corresponding decrease in the yearly yield as well.

It is important to not confuse the simulation in Fig. 4.2 with the yield plot in Fig. 4.3, which is a commonly used plot and can be found in various PV literature, e.g. [30]. Although they may appear similar, this yield plot however only considers the yearly PV yield based on mostly real data and not the power peak values. The yield curve decreases more rapidly from the top towards the edges, which means that orientation is having even stronger effects on yield than on max. power value. Considering for example, an orientation of $0/25$ which according to the diagrams has a maximum achievable power of $0.94\,\mathrm{kW}$ and a normalized clear sky yield of 0.97. When the slope is slightly increased by e.g. $2°$, the peak power value decreases while the annual yield increases. This clearly indicates that, despite appearing to show the same information the two diagrams are actually distinct. If one wants to achieve the maximum annual yield on a limited area, the self-shading of the modules must also be considered. Therefore, it may be advisable to reduce the tilt angle in order to achieve a higher module density on

the surface.

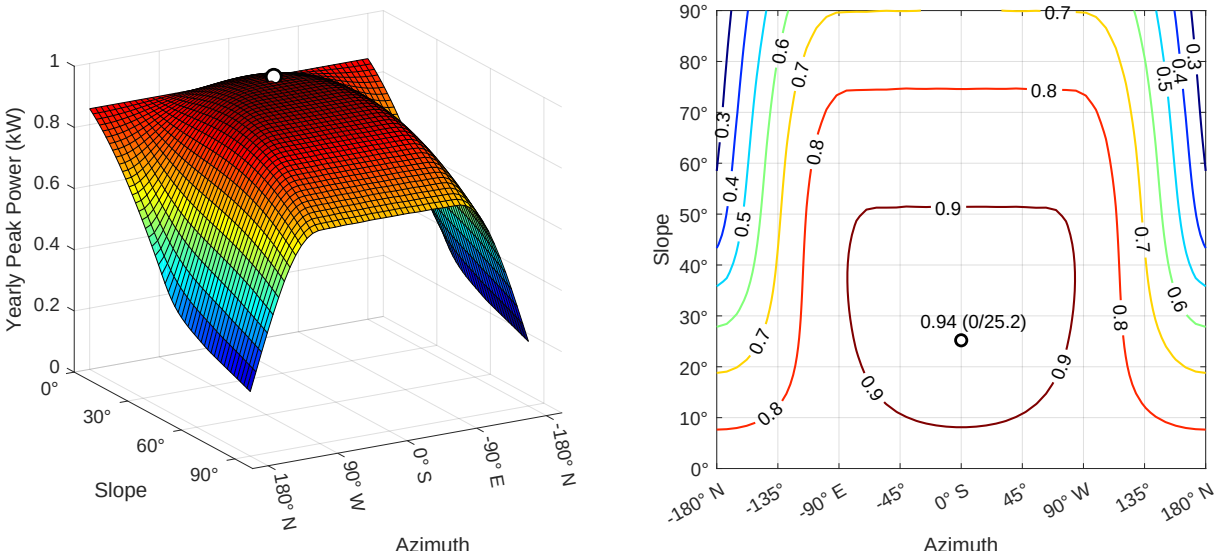

Figure 4.2: Maximum power value that occurs during a year over all orientations.

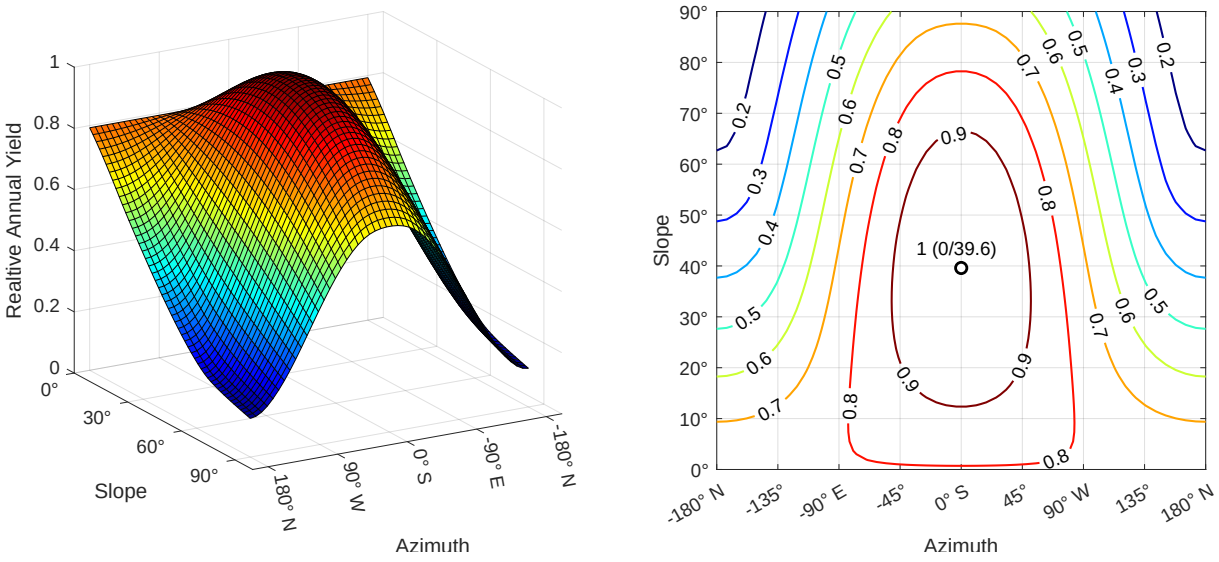

Figure 4.3: Normalized yearly yield plot across all orientations. The yields are related to the best possible orientation in terms of maximizing the annual yield. For Vienna, this is approximately $0/40$, yielding at 2116 kWh for a 1 kWp rated system. Yearly yields are then equivalent to full load hours. Please note that these are clear sky yields. In reality, they would be reduced significantly by approx. 40%, as outlined in section 3.4.

Furthermore, the time when the maximum power occurs has been analyzed for all orientations. For most orientations this is at the time of the summer solstice on 21 Jun, which can be identified on the flat red surface in Fig. 4.4. Only for systems oriented towards the south and tilt angles greater than 30°

other time points become relevant. In these cases the single peak in summer splits up into two peaks symmetrically occurring around 21 Jun. For example, for a $0/40$ orientation, the peaks are both on 30 Apr and on 10 Aug. In the case of a $0/60$ oriented system they separate event more to 29 Mar and 26 Oct. Regarding the time during the day, for steep angles greater than $70°$ and north-facing orientation, the bell curve mutates resulting in showing two peaks for a single day due to the direct sunlight, which is facing the surface on two different times during a day. In the limiting case where $\alpha_M = \pm 180°$ both peaks are of equal height, as can be observed in Fig. 4.4 by the discontinuity when calculating the left-hand and right-hand limits.

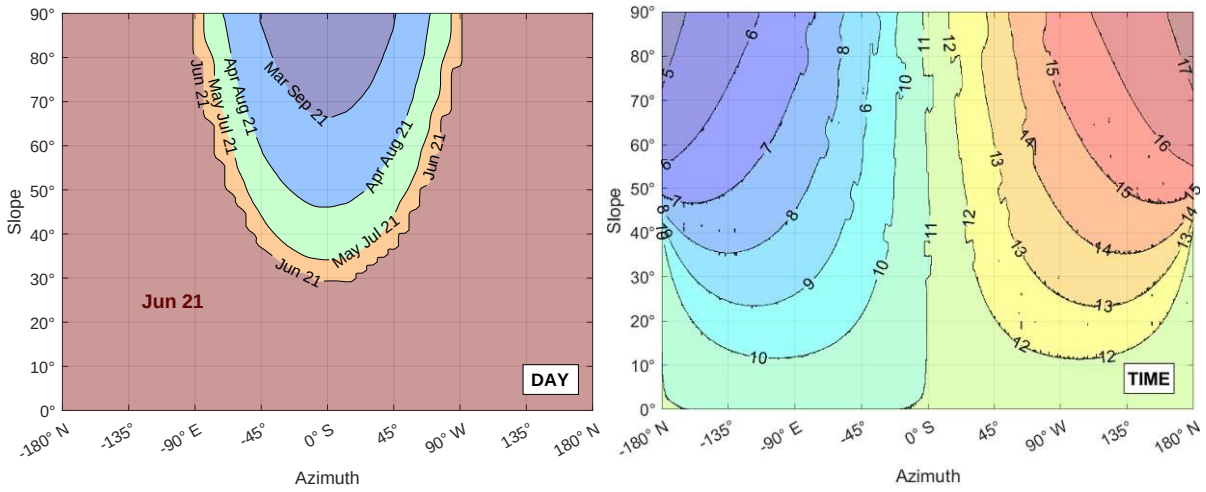

Figure 4.4: Contour plot showing the day when maximum power occurs on a yearly (left) and daily basis (right).

For a single system, the value and time of the maximum possible power that can occur during one year can be derived based on the provided graphs. However, if a system contains two or more different orientations, there is no easy way to determine the maximum occurring power values. In such cases, the max occurring power values need to be derived based on the power curve simulation of the entire system.

4.2 Power Peak Analysis for Multiple PV Systems

When dealing with multiple system orientations each with its given annual peak power, one cannot simply add them together to obtain the maximum achievable power of the whole system because this would overestimate it. Instead, one must consider the individual power curves and the time points when these power peaks occur, both on a daily and hourly basis.

4.3 Impact of Peak Clipping on Different Orientations

Due to the so-called Peak Clipping, peaks are cut off leading to a steady power output during operation whenever the current power would exceed a threshold level. In literature, there is typically a differentiation between *solar clipping* and *inverter throttling*. Solar clipping refers to the power restriction that occurs when PV power exceeds the capacity of the inverter ($P > P_{inv}$). Inverters tend to have an efficiency curve that relies on current utilization. Typically they achieve their maximum efficiency for utilization of approx. $> 95\%$. However, for utilizations below 30% efficiency drops significantly, therefore inverter manufacturers often recommend overloading the inverters by about 20%. Inverter throttling, on the other hand is a feature of inverters in order to manually limit the feed-in power in compliance with any applicable regulations. For example until 2023, Germany had a mandatory feed-in limit of 70% for active power from the rated module power. Now only systems $> 25\,\mathrm{kWp}$ are required to be throttled. In this work the worst-case scenario for the grid (full feed-in with no loads) is analyzed, so there is no need to differentiate between the two terminologies.

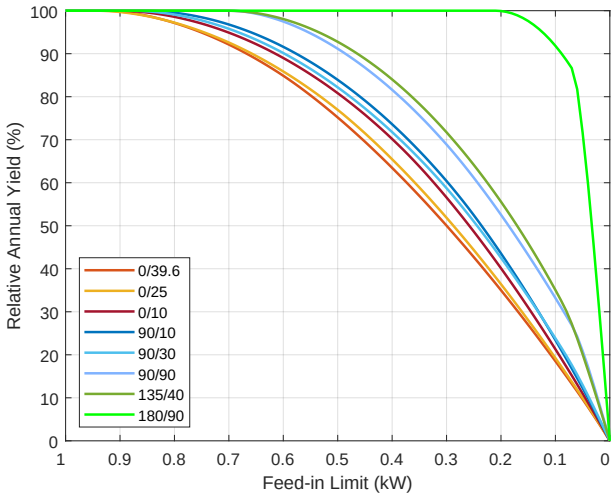

Figure 4.5: Loss in energy yield due to inverter feed-in limit for selected orientations. The yield percentages are referenced to the annual yield for zero inverter throttling. The reddish curves represent south, the bluish curves represent east/west, and the green curves represent alternative directions towards north.

The graphs in Fig. 4.5 illustrate the power loss due to the inverter clipping effect. It does not consider any self-consumption that could be further subtracted from PV power, when considering the grid-related power which would result in upward shifts of the curves. Due to the symmetry between east and west orientations, their impact on the yield is equivalent, thus only the east orientation is considered. The greatest impact of throttling is observed on the worst-case orientation for the grid (lower envelop, orange). The other extreme is formed by a vertically oriented north-facing installation, which

is practically unaffected (upper envelop, light green). However, it should be noted that the normalized annual yield decreases significantly from the orange curve to the light green curve, making these extreme cases largely irrelevant. Therefore, for the majority of actual systems the line will be around the lower boundary curve. For nearly all relevant orientations with high annual yield, the curves show only minor deviations, only edge cases such as facing north with a high tilt angle will show some more noticeable deviations. Limiting the inverter power to $0.5\,\mathrm{kW}$ would result clipping losses of approx. 20%, while at $0.4\,\mathrm{kW}$ there would be about 30% losses, both compared to a nominal PV power of $1\,\mathrm{kW}$. It can be observed that with even with a limitation of $0.7\,\mathrm{kW}$ the power loss in the worst case is at a maximum of just 10%. The point of intersection with the 100% line represents the value in the max. power diagram in Fig. 4.2.

Furthermore this diagram can provide an indication of the practicality of employing an intelligent energy storage system and the extent to which load shading should be carried out when facing limitations in energy supply capacity. It should be noted that the clipping losses, especially in the lower range, are not uniformly distributed over the year but rather are more seasonal or concentrated on a few days within the year.

Chapter 5

Power Grid Simulation

The following sections describe the process of determining the maximal possible PV capacity in a given grid by conducting a Monte Carlo simulation. The method was chosen with reference to the *precise probabilistic approach* (see Fig. 2.1) which forms the foundation for how DSOs calculate the required integration potential on MV level. However, in contrast to the existing calculations, in this work the conducted Monte Carlo simulation is based on the LV grid and explicitly consider the impact of PV system orientation. Based on the simulation results from different orientations and probability distributions in terms of orientation and size of the installed PV systems, results are drawn and should provide a quantitative measure that indicates how important it is for DSOs to have information the orientation data.

5.1 Technical Implementation

The time series simulations are conducted in BIFROST [31] [32], running in a local Docker environment. BIFROST is a simulation and visualization tool for smart energy grids developed by Siemens. The underlying load flow calculations are based on pandapower. BIFROST is built up modularly, where each module represents a specific task such as weather, load flow calculation or e-charging stations etc.

The BIFROST building model already includes a default PV model, however the orientation is chosen randomly by default and is also affected by the weather. Therefore the custom PV model as elaborated in chapter 3, is utilized by employing the BIFROST CSV-feeder module to conduct the simulation. This module enables the feeding of custom time series vectors to any BIFROST dynamic. In this case the pre-calculated PV power curves are then provided to the CSV-feeder module for each PV system separately to perform the load flow calculation. The default weather module is deactivated to ensure that the weather has no influence on the outcome, except for the underlying worst-case temperature curve,

which is implicitly considered within the PV model.

For this work the BIFROST settlement as well as any other simulation parameters, are configured via REST API commands sent by MATLAB, which serves as the simulation execution program. Although BIFROST offers a web-based visual interface, this was only used for debugging purposes in the scope of this thesis. In order to produce reproducible results, the random number generator (which is later used to sample orientation and peak power from a probability distribution) is preinitialized with predefined random seeds. This allows the simulation to be executed with the same parameters at any time, resulting in the same outcomes. It is assumed that all PV inverters generate feed-in power symmetrically, which means that the power utilization for one cable is $P_{\mathrm{PV}}/3$ of the total feed-in power.

5.1.1 Runtime Optimization

The PV model calculates the PV power curves as described in chapter 4 with a 1-minute resolution. The resolution was reduced to $10\,\mathrm{min}$ for the time series load flow calculation, which was necessary to enhance Monte Carlo simulation performance. This effect only applies if the BIFROST sampling time is also reduced to the same value. In the case of *threshold feed-in* the load flow was calculated for only one timepoint, as this is a static problem. To reduce calculation time for *profile feed-in* load flow calculations were performed from 9:00 to 15:00. Although some distinct orientations (especially for $|\alpha_M| > 50°$) might show a peak outside this time window, it still appeared reasonable, as they have a low probability and a branch typically contains several PV systems. Given the worst-case scenario, the peak for entire system still most likely occurs around midday. As computation time is more or less directly proportional to the number of data points, these measures for reducing data points both in resolution and time window size could significantly decrease computation time to approximately $1/30$ of the previous duration, with only a reasonable loss of accuracy.

Another measure, instead of using a sequential search for all nodes, a binary search algorithm is applied, which will be described in detail in section 5.3. This could further reduce calculation time to about a quarter. However, in contrast to the other approaches which scale approx. linearly, the effect of this measure is logarithmic with the grid size. Since all the evaluation is done in MATLAB, and BIFROST serves only as a load flow calculator, the runtime could be further decreased by only exporting relevant dynamics data, including all voltage values of PV nodes and all current values of power lines. The summary of all approaches can be found in section 5.1.1, with speedup factors evaluated through trials using small sample sizes. Nevertheless, they should only offer a sense of the extent to which the different approaches impact performance speedup and are not intended to be precise measurements.

Table 5.1: Impact of different approaches on simulation runtime reduction.

Approach	Speed up factor
Resolution reduction	≈ 8
Binary Search[1]	$3 - 4$
Relevant export	$2 - 3$
Time window reduction	≈ 4

[1] Compared to sequential search, for the used grid size

In conclusion the runtime for one load flow simulation conducted on a PC (8-core AMD Ryzen 7 Pro 5850U with 1.9 GHz and 16GB) takes in averages about 10 s to 15 s for the profile feed-in case. In this scenario the simulation accounts for approx. 80% of the total time, while data export comprises the remaining 20%. Load flow calculation for the threshold feed-in case typically takes between 5 s to 10 s. Each simulation consists approx. $5 - 6$ load flow calculations. Adding everything up results in approx. $(15\,\text{s} + 10\,\text{s}) \cdot 6 \cdot 100 \approx 4$ hours for 100 simulations.

5.2 Grid Configuration

The simulation is conducted in a test grid based on a SimBench grid model [33], which are commonly used in technical publications. It originally came from a research project conducted from 2015 to 2019 in Germany, aimed at creating a simulation database in grid analysis. The advantage is that using standardized grids makes solutions comparable and transparent and offers a benchmark dataset that is suitable for comparing various methods and algorithms. The model grids are not primarily intended to represent existing real networks, instead they should offer a possibility that allows for the investigation of different test scenarios. Another advantage is that it's publicly available and therefore does not rely on any confidential DSO data. The SimBench LV networks are based on statistical data captured from Germany. It should be noted that, especially at the low-voltage level, grids can vary significantly from different localities due to the historical development of the networks. [34] The used SimBench grid covers the low voltage level of the distribution grid. In general all SimBench LV grids are designed in a radial tree topology.

In particular, the SimBench grid type `1-LV-semiurb4-0-no_sw` is used. It's a 400 V low-voltage grid with a semi-urban character, making it more general to cover a wider variety of real network types in DSO grids. This semi-urban grid type consists exclusively of cable connections with lengths

ranging from 1 to up to 60 m, with an average length of about 15 m. As dynamic disconnections are not desired, the version with no switches is used. In the following table 5.2 the grid components are shown which are contained in the SimBench grid with their default specifications, which were then used to parameterize the BIFROST environment. The transformer turns ratio was assumed to be fixed, so tapping was not considered.

Table 5.2: Grid component characteristics.

	Typ	**Parameters**
Transformer	0.4 MVA 20/0.4 kV Dyn5	$S_r = 400\,\mathrm{kVA}$, $I_0/I_r = 0.3\%$
Cable	NAYY 4x150SE 0.6/1kV	$R' = 0.207\,\Omega/\mathrm{km}$, $X' = 0.0804\,\Omega/\mathrm{km}$, $I_{max} = 270\,\mathrm{A}$

The test grid consists of a total of 42 nodes for load or generation, however for this work only generation is considered. The transformer used has a maximum power of 400 kVA, resulting in a maximum power of 9.5 kW per connection point without considering any simultaneous factors or safety margins. Additionally, it's important to note that simultaneous generation and consumption in the network relieve the transformer and the higher-level grid. Although SimBench also provides time series data and standard load profiles for each connection point, the generation data used relies on the introduced PV model. The SimBench specification defines the position of the node in a coordinate grid thus the connections are usually diagonal between nodes, leading to a tree structure in Fig. 5.1. Since BIFROST doesn't support diagonal connections, the corresponding elements were connected orthogonally in the first place. Then, the corresponding line impedances were adapted so that, in total the line has the given impedance.

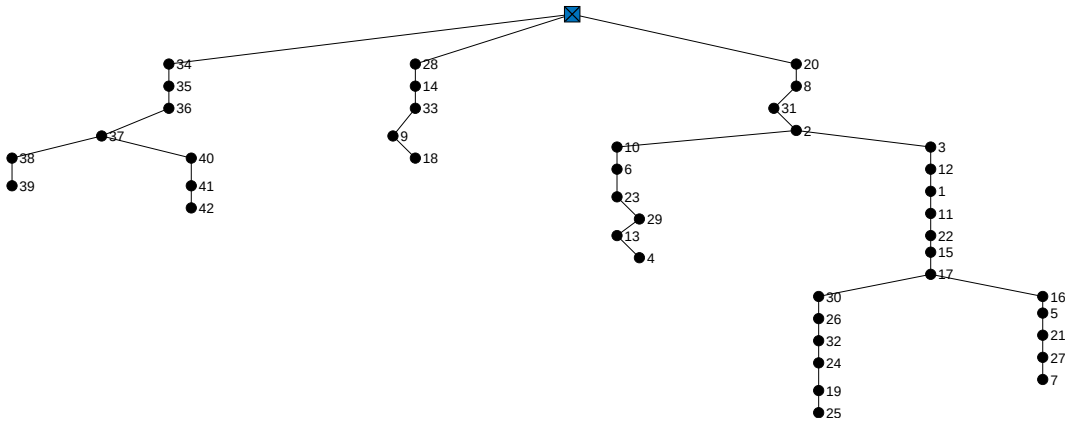

Figure 5.1: Semi-urban SimBench test grid is used for Monte Carlo simulation. The labeling indicate the busbar IDs according to specifications. The cable lengths are not to scale, plotted here because node coordinates and cable lengths are handled separately in SimBench.

5.3 Method

In the following, the method to determine the total PV feed-in capacity of a grid section is explained through an illustrative simulation example. The used approach relies on an adapted binary search algorithm [35], whereas the installed power values considered for all sequentially energized PV nodes, represent a sorted list. This provides the advantage that in comparison to linear search the runtime is largely unaffected by the grid size. The runtime is $\mathrm{ld}(n)\ T_0$, where n represents the total number of PV connection nodes in the grid section and T_0 is the runtime for one day simulation in BIFROST. However, in contrast to binary search which searches for a specific power value in the sorted list, this approach seeks to find the largest element that does not cause any voltage or utilization violations. Thus one must traverse the entire half search-tree, which means the runtime always scales with $\mathcal{O}(\log n)$, in contrast to conventional binary search, which could also achieve $\mathcal{O}(1)$ in the best case if the searched element is in the middle.

As previously mentioned, the method for determining the maximum possible peak power that a grid section can hold relies on a Monte Carlo simulation (MC simulation). A MC simulation is a computational method that uses random samples to estimate outcomes. It involves generating a large number of random scenarios as input and performing calculations based on these inputs in order to aggregate results. It is used in a wide variety of fields including physics, finance or engineering. For this work, a deterministic approach would not be suitable because it would involve solving in a high-dimensional configuration space (considering every possible peak power and orientation on every grid connection point) to gain information about the integration potential. In contrast to this deterministic approach, the MC simulation is suitable if using a large number of random samples. However the random drawing process to obtain these samples is crucial and influences the outcome as discussed in section 5.4.

The blue square on top represents the LV-MV transformer, which serves as the only grid connection point to the higher-level grid. Black nodes depict all possible connection points for a PV system. When a PV system is connected, respectively energized this is indicated by a green node labeled with its threshold power. Red lines show a power overload at a cable, while a red node indicates that the voltage limits are violated (in this case exceeded) at a node. Before running the simulation, in step 0, all power profiles for each nodes are precalculated. This is done since the time required to calculate the load profile, using the introduced model in chapter 3 ($< 1\,\mathrm{s}$) is significantly shorter than the simulation time, which still remains the bottleneck of the whole simulation ($\approx 60\,\mathrm{s}$). All the mentioned runtimes referred to, again relate to the simulations conducted on the same PC as discussed in section 5.1.1.

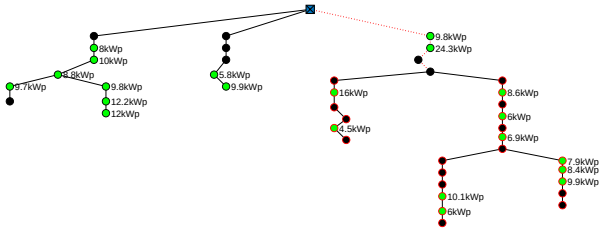

Step 1: Starting with half of the nodes $21/42$ randomly energized with random load profiles. As both voltage and utility violations are observed, the new subset is reduced to the left half (smaller total power values) of the ordered node set. In the next step $\lfloor \frac{1+21}{2} \rfloor = 11$ nodes are energized. Total installed power: $204.6\,\mathrm{kW}$.

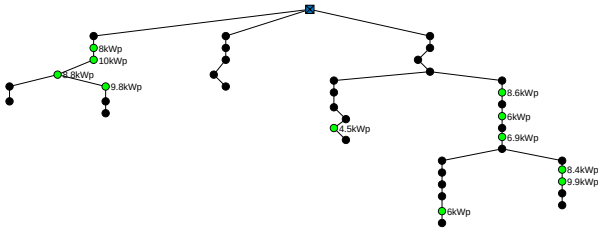

Step 2: Load flow calculation for one day with now 11 nodes energized. The orientations and threshold powers remain unchanged, the number of active PV nodes is halved. As no violations are occur, the number of active PVs is increased to $\lfloor \frac{11+21}{2} \rfloor = 16$, in the next step. Total installed power: $86.9\,\mathrm{kW}$.

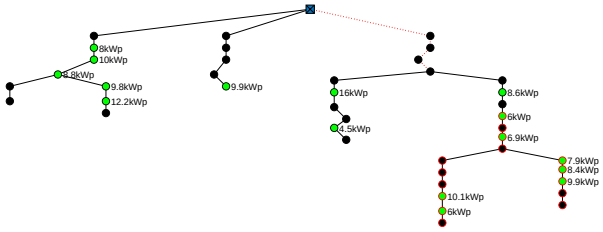

Step 3: 16 nodes energized. Load flow simulation again results in both voltage and utilization violations. Continuing with $\lfloor \frac{11+16}{2} \rfloor = 13$ nodes in the next step. Total installed power: $143\,\mathrm{kW}$.

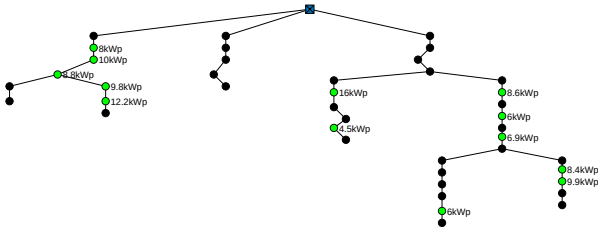

Step 4: 13 nodes energized, no violations. Increasing the number of energized nodes to $\lfloor \frac{13+16}{2} \rfloor = 14$ in the next step. Total installed power: $115.1\,\mathrm{kW}$.

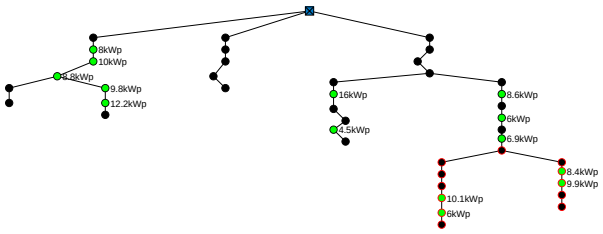

Step 5: 14 nodes energized, resulting in a voltage violations at the end of the right feeder. The total installed power is $125.2\,\mathrm{kW}$. The algorithm terminates as the load flow calculation for 13 energized nodes has already been performed with no violations.

As demonstrated above, in this example with randomly preselected time series it is shown that the maximum PV potential is reached when 13 PV nodes are energized, leading to a maximum power of $115.1\,\mathrm{kW}$. For this particular grid, the algorithm generally terminates after $\mathrm{ld}(42) = 5.4$, which results

in either 5 or 6 steps. This simulation example was conducted for the case where the orientation of each PV system is known and explicitly considered, referred to as *profile feed-in*. The same simulation is then performed for the case where orientation data is unknown and it is assumed that each PV system feeds in with its threshold power, denoted as *threshold feed-in*. In this scenario, the maximum number of energized nodes where no violations occur is at 12, leading to a total installed PV power of 99.1 kW. Consequently the resulting additional potential for this case with $N = 1$ simulation would be 16%. However, since this number is only based on a single simulation, it is definitely not meant to be representative. It just serves to show the working principle of the method. In the context of the Monte Carlo simulation, the simulation is then conducted N times for both the *threshold* and *profile* feed-in case to capture a large range of possible grid configurations and derive the overall distribution.

Code 5.1: Implementation of the main file as simulation controller. The actual simulation, data generation and checking for violations are implemented in the corresponding subfunctions.

```
NAME = "demo";                % name of settlement
NUM = 300;                    % number of simulations
GRID = "simbench_semiurb4"; % gridtype: rural1, rural2, rural3, semiurb4, semiurb5, urban6
DIST = "mastr";               % pdf: mastr, yield, uni, threshold, bifac
POWERCLIP = 100;              % peak clip in percent

rng(99); % set seed key
nameID = NAME + "_" + GRID + "_" + DIST + "_" + POWERCLIP;
path = "results\" + nameID; if isfolder(path), rmdir(path, 's'); end, mkdir(path);

runInfo = bifrost_buildGrid(nameID, GRID, runInfo);  % build settlement in BIFROST.

for sim = 1:NUM
    for testcase = ["threshold" "profile"]
        if testcase == "threshold"  % precalculate all generation profiles
            pool = bifrost_createCSVprofiles(runInfo, "threshold", POWERCLIP);
            startHour = 12; endHour = 12.5;
        elseif testcase == "profile"
            pool = bifrost_createCSVprofiles(runInfo, DIST, POWERCLIP);
            startHour = 9; endHour = 15;
        end

        runInfo.currentSimulation = sim;
        runInfo.testcase = testcase;

        left = 1; right = runInfo.nodes;
        while (right - left) > 1  % binary search
            active = floor((left + right) / 2);  % energized pv systems
```

```
29
30            pool = bifrost_updateCSVprofiles(runInfo, pool, active); % add or reduce PVs
31            runInfo.currentPool = pool;
32
33            % run one monte carlo iteration for 21 jun (day 172)
34            violation = bifrost_simulate(nameID, runInfo, 172, startHour, endHour);
35
36            if violation == "0"  % no violation -> take right
37                power = sum(pool.peakpower .* pool.energized);  % total active peakpower
38                connectionpoints = active;  % number of PVs
39                left = active;
40            else % violation -> take left
41                right = active;
42                violationtyp = violation;
43            end
44        end
45        % save results
46        RESULT.(testcase).power = [RESULT.(testcase).power power];
47        RESULT.(testcase).conpoints = [RESULT.(testcase).conpoints connectionpoints];
48        RESULT.(testcase).violationtyp = [RESULT.(testcase).violationtyp violationtyp];
49    end %testcase
50        save(path + "\RESULT", "RESULT");
51 end %sim
```

The voltage deviations at each grid connection point in the LV grid must be limited to within $\pm 10\%$ of the nominal voltage [36], which has to be ensured by the DSO. To account for possible voltage fluctuations in the higher level grid, for the simulation the violation threshold is set to be 5% assuming that the voltage of the LV-MV transformer remains fixed.

5.4 Probability Distributions of System Parameters for MC Simulation

The PV systems were sequentially integrated into the grid one by one. The calculation of the power curves relies on only three parameters: P_{r}, α_M and θ_M, which represent a configuration space of all theoretically possible generation profiles. When a new PV system is placed into the grid for the MC simulation, each of the parameters is chosen randomly based upon the probability density functions in Fig. 5.2, which will be described in detail in the following. In order to obtain realistic results the random drawing process is performed with three different scenarios, which will be later discussed to determine if these distinctions actually make any difference.

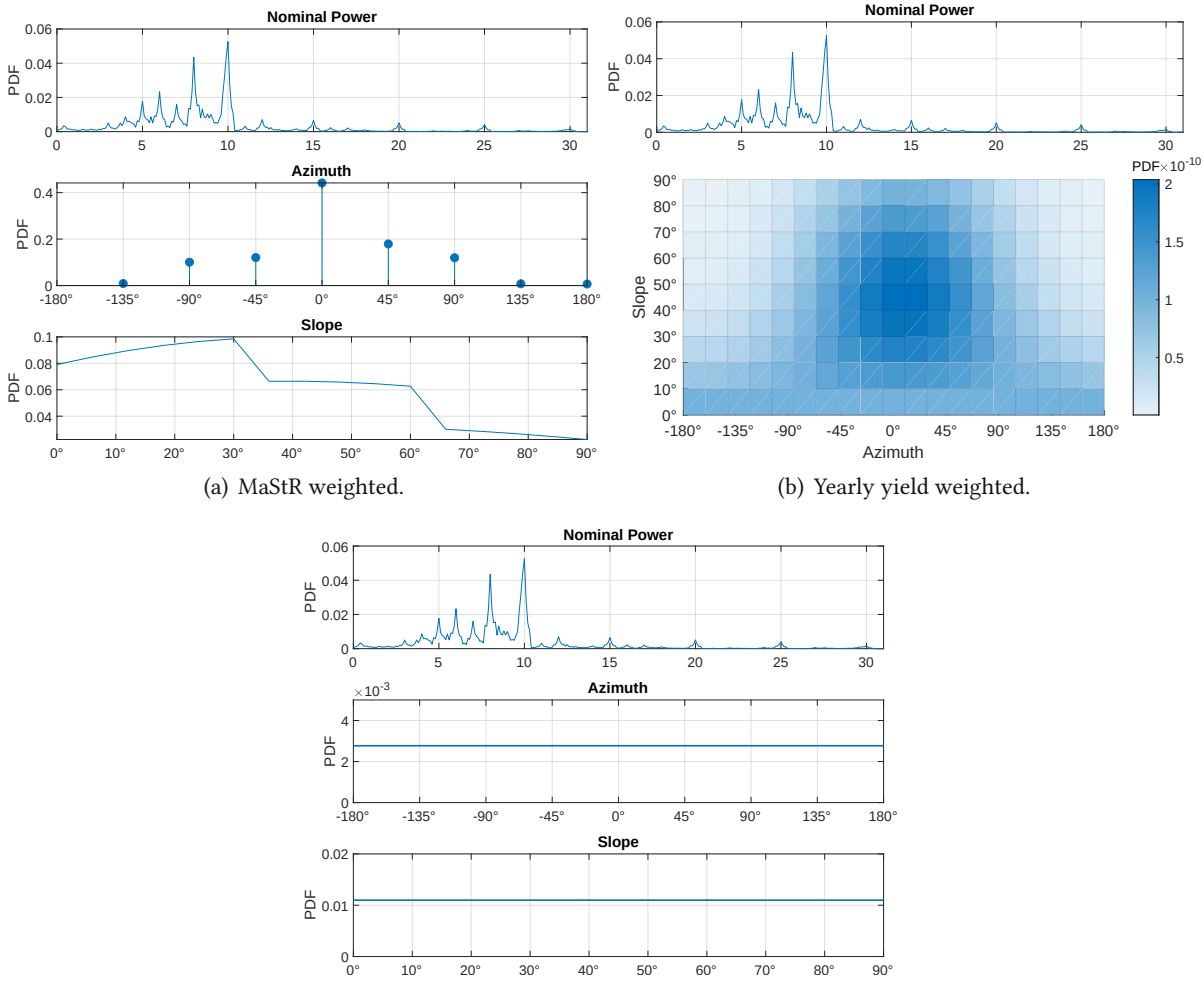

(a) MaStR weighted.

(b) Yearly yield weighted.

(c) Uniform distribution.

Figure 5.2: Different probability density functions (PDF) used in MC simulation. The nominal power distribution is always taken from MaStR and is the same for all three scenarios. Nominal power data in the range of 0 to 100 kW is used, however except for a small peak at 100 kW, the segment > 30 kW is negligible and therefore not plotted.

The density function for the nominal peak-power distributions for all approaches is extracted from the German Marktstammdatenregister (MaStR) [4] based on a data export from Jan 2020 to Apr 2022. It is determined by *NettonennleistungDerEinheit* which corresponds to the threshold power as the minimum of inverter and the PV peakpower. While this represents a reliable approach, it has the drawback that political incentives may lead to a distorted representation which is not necessarily based on technical or scientific considerations. As can be seen in Fig. 5.2(a), certain distinct peaks can be identified. The large peak at 10 kW can be explained by being a tier for EEG compensation[1]. PV system owners in Germany are compensated based on fixed feed-in tariffs, with reduced rates for systems larger than

[1]The EEG levy is an additional fee paid by all energy consumers in Germany on top of the electricity price to compensate for renewable energy tariffs. The EEG levy has been eliminated in 2022.

$10\,\mathrm{kWp}$. Additionally gains through feed-in compensation are exempt from income tax, and producers were also not required to pay the EEG compensation on self-consumed power. Therefore, almost all of the existing systems connected to the LV grid are aggregated in the $< 10\,\mathrm{kWp}$ section. For the other peaks occurring at 5, 6 and $8\,\mathrm{kWp}$ as well as smaller ones at 15, 20, 25, and $30\,\mathrm{kWp}$ no special explanations have been found. However, they might arise from regional tiered PV subsidies where a higher budget is only available if a certain peak power is reached. With 2023, all these thresholds have been raised to $30\,\mathrm{kWp}$, although this is not represented in the data yet, but it is expected that the accumulation of systems with $< 10\,\mathrm{kWp}$ will loosen up the future, also because of the generally higher electricity prices, which also create a trend toward larger installations. Due to these arbitrary accumulations resulting from certain regulations which may only be true for a specific time period or region, a mean filter was applied with a window size of $0.7\,\mathrm{kW}$ to minimize this effect to some extent. This window size showed good results without excessively manipulating the original data. Nevertheless the nominal power probability distribution is expected to be not as relevant as the orientation for the MC simulation because over a large number of simulations they tend to average out.

MaStR weighted PDF: In the first approach the data is based on existing specifications, obtained directly from MaStR. The main azimuth orientations are fully available in MaStR, clustered in $45°$ batches thus data was extracted from this source. Main orientation assigned as East-West was equally split, with 50% facing east and the other 50% facing west. Subsequently data was normalized to create a proper probability density function. While slope data is also available in MaStR, it unfortunately cannot be exported on a large scale, therefore another approach had to be used here. Basically the slope probability density function was derived by considering the yield for $\alpha_M = 0°$ (south orientation). This means that a high yield, e.g. at $30°$ also leads to a higher probability density for that angle. To account for practical feasibility, the PDF was additionally weighted with a solar-potential coefficient based on the roof tilt angle. The weighting coefficients are 3 in the range $0°$ to $30°$, 2 for $30°$ to $60°$ and 1 for tillt angles between $60°$ to $90°$ following a slightly adapted roof-potential analysis in [37].

Yearly yield weighted PDF: In this scenario, the weighting coefficients are determined based on the results calculated in Fig. 4.3. The total yield function is squared and normalized, otherwise it would be too similar to a uniform distribution. The advantage of the continuous 2D joint probability distribution, compared to the first approach, is that it also accounts for the fact that for south-oriented modules smaller angles are more favorable, while for east/west-oriented systems larger angles are more beneficial. In the previous approach the random drawing of azimuth and slope had been considered independently.

Uniform distribution PDF: The aim of this method is not primarily to determine the maximum PV potential in the grid, but rather to investigate the actual relevance and influence of the presented PDFs on the simulation results. It consciously overemphasizes the number of PV systems with orientations in secondary directions which in reality wouldn't be implemented on a large scale to such a significant extent. Thus it should be used for validation purposes and should also clarify whether a significantly larger amount of power can be integrated into the grid.

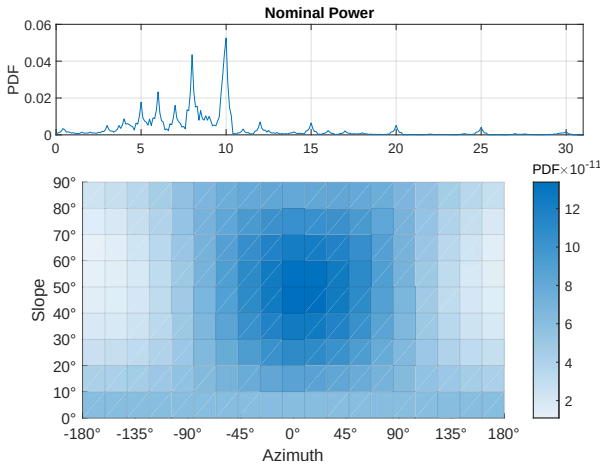

Figure 5.3: Yearly yield weighted PDF for bifacial PV modules.

Bifacial distribution PDF: With Fig. 5.3, this method should additionally investigate the influence of upcoming bifacial modules. It is also weighted according to yearly yield, with the assumption that it involves only bifacial modules following the model from section 3.5. Compared to monofacial modules, the area with an angle of less than $45°$ has similar a structure. However, the region for steep tilt angles is much more beneficial now, suggesting that this approach will integrate a larger number of steep PV modules, thus it is expected to have a positive impact on the integration potential. Although only bifacial modules are considered, for small slope angles bifaciality primarily affects the overall efficiency rather than the shape of the generation profiles. Thus it was omitted to add an additional share and explicitly consider monofacial modules in that case.

5.5 Simulation Results

In the following, the solution of the MC simulation is described and discussed. All simulations were conducted for $N = 300$ iterations. This means that the random PV integration process as described in section 5.4 is performed 300 times, resulting in 300 different maximum possible power values for the investigated grid. These power values are then arranged in ascending order, where P_i represents an element in the sorted list. Consequently this array is formed from the lowest to the highest total

integrated PV power that the grid can hold without violations. The lists are subsequently plotted as graphs for each case, providing a better understanding of how much variation there is or whether the results are consistent.

In a first approach the 80% quantile was used by simply taking the 240th value of the sorted list to determine the total PV integration potential. This was based on the assumption that the upper 20% of power values are already less consistent and would lead to an overestimation. The regulations [9] even suggest using the 99.5% quantile, however this can't be directly compared because this advice is based on real data measurements and abnormal cases aren't expected to occur to the same extent as in the simulation. Nevertheless, it's also mentioned that special occasions can be examined from the dataset if properly documented. Considering the placement of a large PV system in the simulation, with high nominal power but bad orientation (e.g. facing north with a steep angle). In this scenario, even in the worst case over the course of a year only around 30% of the nominal peak power can be achieved. In practice, the installation of such systems wouldn't be considered because, even if all the energy is self-consumed it wouldn't be economical. However, in the case of the Monte Carlo simulation these abnormal cases, although having low probability, can still appear when using large number of samples N. Consequently, in addition to the simulation's limited resolution and outliers, these abnormal cases may be present in the captured data and can distort the results. A possible solution could involve to exclude cases lower than a certain threshold in the probability density function, which would lead to more consistent outcomes. In this work, a different approach was chosen to eliminate inconsistent data after the simulation. Subsequently, the maximum integration potential is determined by taking the mean value over all sorted simulations

$$\sum_{i=0.1N}^{0.9N} P_i \tag{5.1}$$

while excluding the upper and lower 10% of all data values, which is also referred to as the *trimmed mean*. This approach has the advantage of being very robust against any outliers. The usage might also be justified for the reason, as most of the extreme edge cases probably only occur in simulations and are unlikely to happen in practical situations since DSOs can also actively counteract such situations. For example, if a very large PV plant is constructed at the beginning of a line, it could lead to immediate full grid utilization in the simulation, however in reality it most likely wouldn't be approved by the DSO on LV level.

The resulting graph from the MC simulation of the first scenario, where the placement of new PV systems is according to Fig. 5.2(a) is depicted in Fig. 5.4. The feed-in capacities determined in in each

individual MC iteration range from almost no feed-in power to an allowed feed-in capacity of approx. 200 kW. As expected, for the calculation method where no orientation data is provided the total PV capacity in the test grid is lower, hence the threshold feed-in curve represents a lower boundary in the diagram. It is also noticeable that the threshold feed-in curve is more constant compared to the profile one because it is not influenced by the probability distribution of the orientation parameters but only by the random nominal power distribution. As the nominal power PDF stays constant across all scenarios (*MaStR*, *Yield* and *Uni* distribution) the threshold curve is expected to remain uniform for all three scenarios. However in order to check for consistency, the threshold curve was recalculated with a different random seed. Consequently, when comparing the resulting curves they show hardly any difference. This will be briefly addressed in section 5.5.2 later.

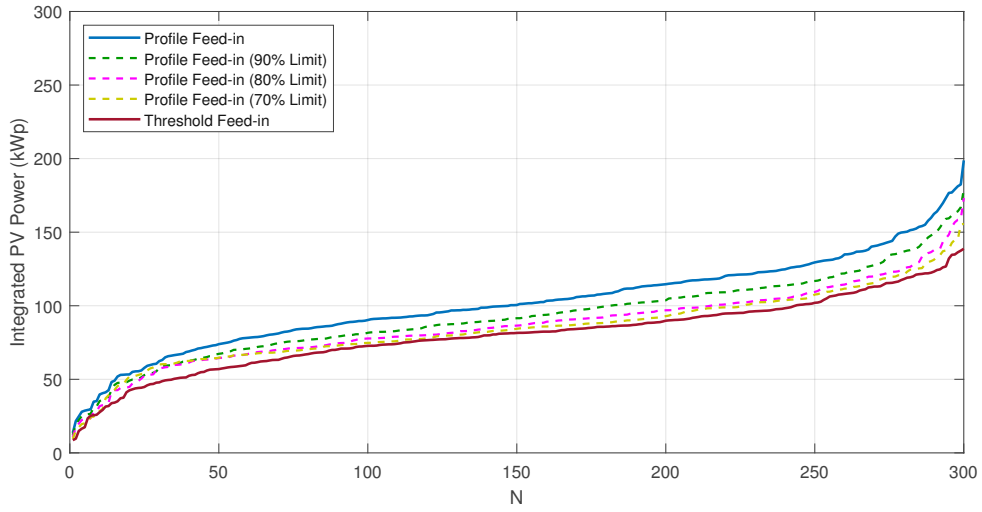

Figure 5.4: MC simulation result based on MaStR weighted PDF.

The upper blue curve in Fig. 5.4 represents the sorted results of the Monte Carlo simulation considering the distinct generation profiles. The dashed lines, on the other hand denote the solutions while taking a feed-in limit into account. The feed-in limit could refer to either an inverter with a lower nominal power than the module peakpower as discussed in section 4.3, but can also be interpreted as a general adjustment factor used by the DSO for grid calculations. The power values in the plot correspond to the already reduced power values ($P_\mathrm{r} \times LimitFactor$), hence the dashed lines are below the profile curve, which might seem counterintuitive at first, because it would be expected that a feed-in limit enables more power to be integrated into the grid. However, as mentioned these values are associated with the reduced power values. Further reduction of the limit implies that even more PV systems can be installed, pushing the dashed line closer to the threshold feed-in curve as the clipped generation profiles become more similar to the threshold curves.

At first, it may appear that the curves are only shifted along the y-axis, but this is not the case. Considering $N = 50$, the relative difference is 34% and for $N = 250$ it is about 50% which proves the opposite. The contrast between *threshold* and *profile* feed-in becomes even more noticeable at the boundaries where the left edges of the curves align and then significantly diverge on the right side. It can be generally observed over in the further simulations that the curves diverge even further for higher values of N. Whether this effect disappears with a larger number of interartions cannot be determined as it has not been tested. Nevertheless, this issue is effectively avoided by not using point evaluations for determining the integration potential, but instead applying the average as showed in (5.1).

In this first scenario on average 12 out of the 42 possible grid connection points one where energized. When analyzing the causes of violations, it becomes apparent that voltage issues are the major bottleneck. In about 45% of the simulation cases, upper voltage band violations were the limiting factor, whereas only 16% of the simulations were terminated due to thermal utilization limits. Approx. 40% of all cases showed both voltage and overload issues. These number highlight the significant relevance of voltage issues, especially in the case of the used semi-rural test network. Nevertheless, it should be noted that these figures are evaluated for a selected voltage limit of $\pm 5\%$ and would vary substantially when changing the voltage violation threshold.

This paragraph briefly summarizes the results obtained from the MC simulation presented in Fig. 5.5 with yield weighted PDFs. Comparing the results with the previous MaStR scenario, the curve's shape and structure is similar to the previous example. Evidently with this weighting a greater PV power potential is achieved in the grid, while the threshold curve remains almost unchanged. Furthermore an overlap for approx. $N < 5$ can be observed in the diagram. This occurs because the sorting has been done individually for each data vector, meaning that the values for each individual N do not have to be from the same MC iteration. However values in this range are not averaged anyway. The number of grid connection points and the ratio between voltage violations and utilization overloads are almost equal to the previous scenario.

When using the unified distribution of orientation parameters in Fig. 5.6, the integration potential significantly increased throughout all iterations. This confirms the hypothesis and shows clearly that the choice of the right PDFs is crucial and has significant impact on the solution. On average, approx. 4 additional PV systems with about $30\,\mathrm{kW}$ in total could be integrated more compared to the previous scenarios. There was no change in the violation ratios.

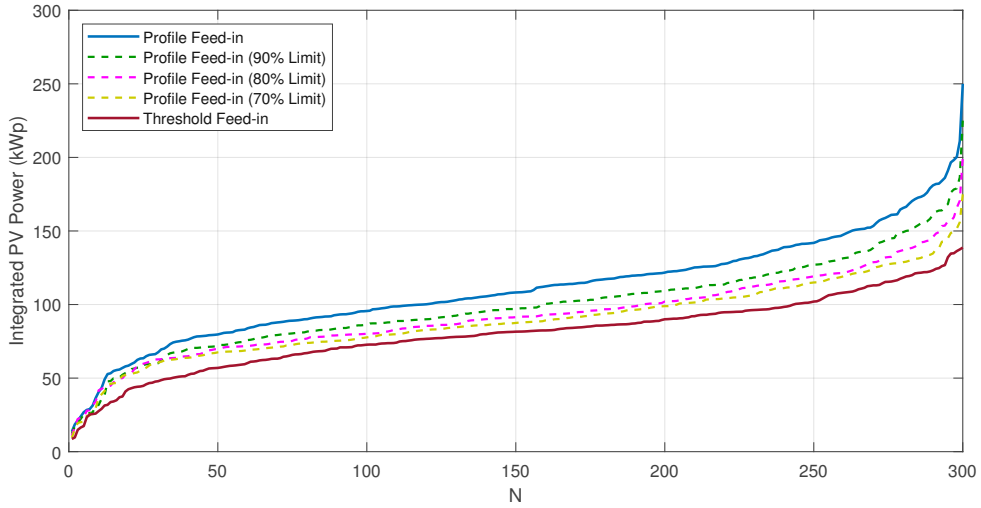

Figure 5.5: MC simulation result based on yield weighted PDF.

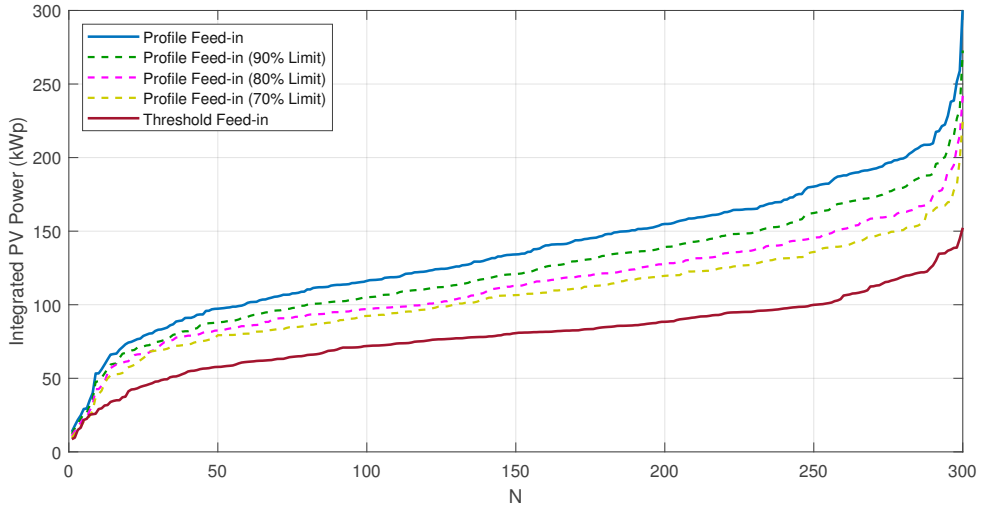

Figure 5.6: MC simulation result based on uniformly weighted PDF.

In Tab. 5.3, all results of the conducted scenarios described above are summarized once again providing an overview of the outcomes. Assuming that the DSO does not consider any reduction factors, there is an additional PV potential of 23% in the MaStR case and 33% in the yield case. This extra potential, of about one quarter to one third of the total installed power, basically arises just from the lack of orientation information leading to differences between the calculations and the actual maximum values which could appear in reality. According to information provided by an expert feedback round conducted on 14 Sept 2023 some DSOs in Austria perform calculations only with threshold power values and assume a general reduction factor of 0.8, but only at the MV level. When considering the complementary values of the resulting numbers, 77% and 67%, as estimates, it becomes evident that the DSO's estimation is indeed justifiable and and rather conservative. However, it is important to note that a general reduction

factor is only applicable at higher gird level, where multiple PV systems are installed. For a small grid segment, e.g. with only 5 systems the assumption of 0.8 may potentially underestimate the total power as in this small branch it is indeed likely possible that all systems are optimally aligned.

Table 5.3: Comparison of key results from MC simulation on total feed-in potential in the SimBench testgrid. All data in kW.

		Threshold Feed-In	**Profile Feed-In**					
			MaStR		Yield		Uni	
Feed-In Limit	100%	82.6	101.7	**+23.1%**	109.7	**+32.9%**	136.1	**+64.8%**
	90%	79.7	92.5	**+16.1%**	98.4	**+23.5%**	122.8	**+54.1%**
	80%	81.1	86.9	**+7.2%**	92.3	**+13.8%**	113	**+39.3%**
	70%	82.4	84.8	**+2.9%**	89.2	**+8.2%**	106	**+28.7%**

Since the threshold case remains unaffected by the feed-in limit, it's only relevant in the case of profile feed-in. Hence, the first column which presents the threshold feed-in power values from four independent simulations, all are yielding to approximately the same outcome of about 81 kW. Comparing the figures for MaStR and yield weighting, they clearly show a consistent trend though with some differences. Determining the definitively correct approach remains uncertain, as both scenarios have their respective justifications. Taking the feed-in limit into account, it can observed that it reduces additional power potential. At around 70%, the additional power drops to less than 10% and at this point, it likely would not be worth the effort to capture orientation due to the low benefit. Additionally potential model uncertainties has to be considered such as extreme temperature variations or imprecise orientation data. The results for the unifrom distribution case generally highlight the influence of distribution functions, but were not further considered.

5.5.1 Consideration of Bifacial Modules

The same MC simulation was conducted using the bifacial model. The probability distribution for orientation is yield-weighted only, because of the limited availability of statistical real-world data as of now. The evaluation in the threshold case was carried out using the STC power values of each module, where the nominal power from the distribution is considered as the STC value of the module front side. In total, 117 kW could be installed indicating additional PV integration potential compared to the threshold calculation of approx. 47%. This high value is a result of the grid-friendly generation profiles. Furthermore, the total yearly energy production in the grid, which was not considered in the simulation, would also be higher due to the bifacial gain. In contrast to the monofacial simulations, where cable utilization accounted for 10% of the total violations, it nearly doubled, increasing to almost 20%. However, voltage violations still the remain the predominant limiting factor.

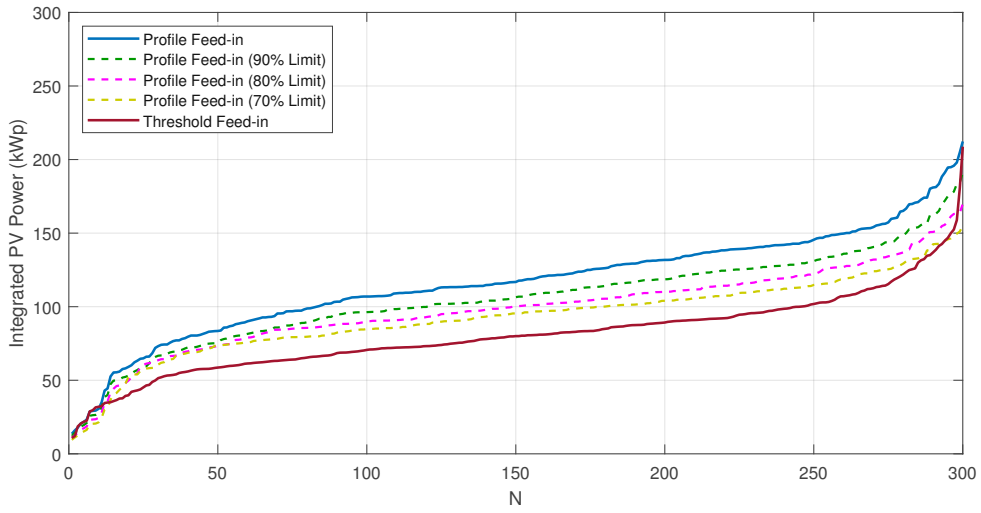

Figure 5.7: MC simulation result based on bifacial yield weighted PDF.

Overall, obtaining individual orientation information is highly advantageous for bifacial modules due to the complementary generation profiles. While the numerical outcomes in Tab. 5.4 seem promising, it is important to consider that predicting generation profiles for bifacial modules can be more challenging due to factors such as the impact of environmental reflectivity and presence of various technologies with inconsistent power specifications. The deviations in the threshold feed-in column in the range $< 1.2\,\mathrm{kW}$ may result from the limited number of Monte Carlo iterations.

Table 5.4: Comparison of bifacial module results from MC simulation on total feed-in potential in the SimBench testgrid. All data in kW.

		Threshold Feed-In	**Profile Feed-In** Bifacial	
Feed-In Limit	100%	79.8	117.4	**+47.2%**
	90%	80.4	106.2	**+32.1%**
	80%	81	99.4	**+22.7%**
	70%	80.2	94.1	**+17.3%**

5.5.2 Convergence

This section briefly discusses the selection process for the number of iterations and whether it is suitable for evaluating the integration potential. The curves in Figs. 5.4 to 5.7 do not converge as they do not tend toward a single value. For example, as N approaches infinity the graph will not tend towards a single power value, but instead the curve gradually approaches a characteristic curve which is specific to the investigated grid and the used distribution functions. The shape of this characteristic curve also contains information about the structure of the network. A concentrated grid with few connection points would have a relatively constant curve, whereas a grid with two feeders where PV nodes are equally distributed would show a variable curve. However individual data points within the sorted lists do indeed converge and therefore for example the 50% quantile remains constant using a high number of simulations. In Fig. 5.8 the selected trimmed mean value is plotted across the course of conducted MC iterations over time. It shows that the limit is reached already after roughly 100 simulations. Consequently, it can be assumed that a sufficient level of accuracy can be achieved for $N = 300$.

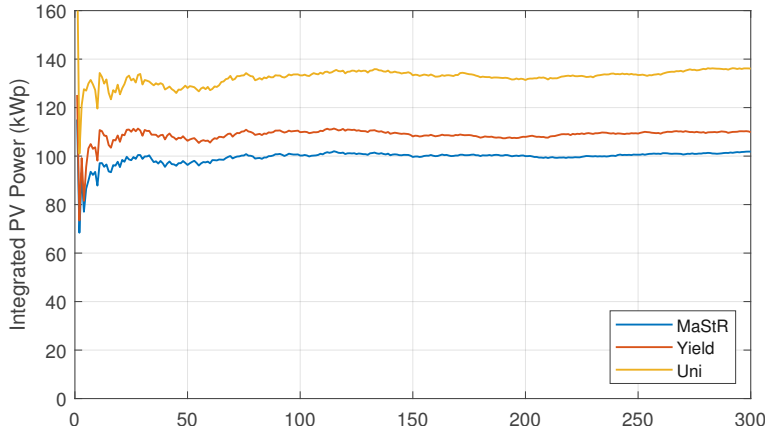

Figure 5.8: Estimated PV power pontential over the total number of MC iterations.

Additionally an estimation of convergence was performed using the threshold curve, which was recalculated under identical conditions with a different random seed. The mean deviation between these curves consistently remained below 5% at all time points, indicating that the curve actually converges toward its characteristic curve. This is also evident in the threshold columns in Tabs. 5.3 and 5.4.

5.6 Discussion

To structure the results, the terminology is recapitulated, emphasizing how this might benefit customers and DSOs in the future. Currently, only the *threshold feed-in* approach can be utilized, as orientation data is unknown. Thus DSOs can only assume the worst-case scenario, considering that inverters feed in with their nominal power. Potentially in future, the *profile feed-in* curves will enable more accurate assumptions. Hence in this simulation, orientation data is taken as known, which allows that the distinct generation profile of each system can be considered. Since DSOs do not cover orientation data in their grids, they had to be assumed by the distribution functions (MaStR, yield or uniformly weighted) presented in section 5.4. According to the proposal in Fig. 5.9, the profile feed-in curve could also be interpreted as grid-related power, as the PV system cannot exceed the precalculated curve at no point in time. Therefore, it would provide a more specific indication than the constant peak power of the modules or the threshold power. Whether using the orientation data just for reporting to the DSO or implementing it directly on site (with a controller which could potentially reduce PV power or increase consumption) exceeds the scope of this work.

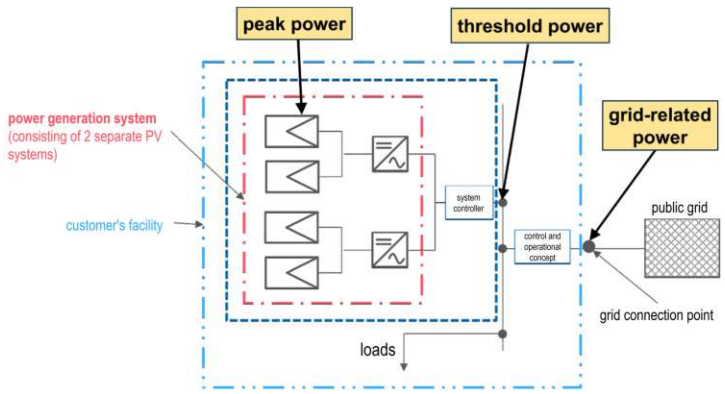

Figure 5.9: Adapted from E-Control [18]. Initially, this proposal aims to additionally consider storages or consumption together with produced energy. However, with a known orientation the control unit could also take into account the maximum expected generation profiles.

The outcomes of the conducted simulation result in an integration potential in kWp, indicating the maximum nominal module power that can be installed within the investigated grid. While the yearly yield for the network wasn't explicitly captured, it can be assumed that with a sufficiently large number of PV systems, the yearly yield would also increase by a corresponding percentage. This is because the additional power, unlocked through the consideration orientation data, is also drawn from the same density function. Consequently without considering a feed-in limit, an additional yearly yield of 23 to 33% can be expected across the entire grid.

5.6.1 Limitations and Distribution of Violations

The causes that ultimately limited the addition of further PV systems, leading to the simulation termination, have already been partially addressed in the specific test cases. The following comparison in Fig. 5.10 summarizes how violations are distributed using different distribution functions. In every MC iteration, the violations limiting the integration of more PV systems were recorded and subsequently statistically analyzed. Voltage violations dominate in the investigated SimBench grid with approx. 40%, which however largely depends on the chosen voltage limit of 5%. Changing the voltage limit would lead to a notably different distribution of violations cases, therefore these figures should not be overinterpreted.

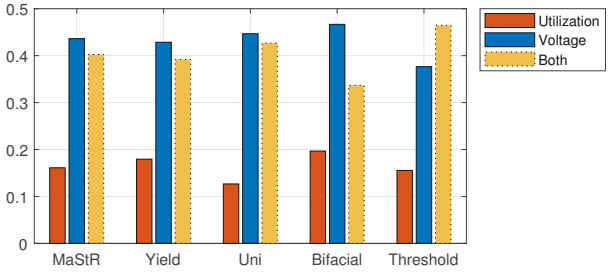

Figure 5.10: Distribution of the causes limiting the integration of additional PV systems for each testcase. The threshold case was averaged out over all simulations conducted for the threshold profiles.

5.6.2 Other Methods for Increasing the Integration Potential

In the following additional comments are made, which have already been covered in the mathematical fundamentals in chapter 2 but were not considered in the simulations. The simulation results indicate that just by accurately capturing all power generation profiles in a grid, it becomes possible to increase the total installed PV capacity. But apart from this passive approach of increasing the integration potential, active methods could be also considered. In the investigated test grid, voltage problems were the primary limiting factor. To address voltage problems there are active approaches, such as using an On-Load Tap Changer or enhancing the reactive power control, which in the best case is leading to completely eliminating or minimizing voltage violations, leaving only utilization problems to consider. The issue of thermal line overloads can be addressed through intelligent dynamic power control which is currently in ongoing discussion [38]. With this measure, DSOs could demand that PV owners reduce their feed-in power or shut down completely if the current grid situation requires it due to weather conditions or during periods of low consumption. These mentioned methods are promising but require a physical upgrade of the grid (installation of measurement points, new transformer and communication interfaces), while the approach addressed in this work can be seen as purely passive.

Chapter 6

Outlook

The results of this study indicate that the knowledge of PV system orientation can certainly help on optimizing power grid utilization. Within this work the simulation utilized current data concerning both PV technology and the local weather in Vienna. Nevertheless, it cannot be ruled out that, due to extreme events such as low temperatures in summer, the long-term increase in solar intensity or unnatural reflective occurrences that cannot be generally modeled, there may be higher possible power values. These factors will have to be considered with an adequate safety margin in advance.

In this work the orientation of a PV system was assumed to be fixed and precise, while the method for acquiring this orientation data is not addressed. However, in practical scenarios obtaining viable orientation data for systems can be challenging. For new installations this could be overcome by including orientation details within the installation documentation form. The installation document contains basic information about the system and is filled out by the electrical installer, in which he must ensure that the installed system meets requirements regarding inverter type, max. threshold power or safety. But significant inaccuracies between the information provided and reality cannot be ruled out here either. Including additional orientation information in the installation document, however contradicts the requirements set by PV interest groups, which demand reducing the level of detail in submission documents to the necessary minimum [39]. Nevertheless it should still be considered acceptable in light of ongoing grid congestions, if this information enables new PV capacities. Alternatively this could be achieved by using a smartphone app that could be prescribed by the DSO to obtain roof azimuth and slope through smartphone sensors during the installation process. Furthermore, this app could potentially replace the conventional installation document. Although other commercial solutions exist with specialized devices to collect roof information, they are clearly not practical for large-scale implementation.

In contrast to newly installed systems, investigating solutions for acquiring orientation data from existing systems in future research could be useful in depicting the current grid status. One possibility is obtaining orientation data from smart meter power curves. This solution would likely require data with a minimum 5-minute resolution and a data length at least one week. The major advantage is that it could be automated and doesn't require any additional devices. However, data protection remains an unresolved concern, as DSOs typically lack access to personal data. Alternative solutions that could be implemented relatively quickly on a large scale might involve satellite-based data or the usage orthophotos captured by UAVs. But these approaches could potentially be less accurate and may require additional human editing.

An alternative strategy could involve configuring a threshold power curve instead of a fixed threshold power value within the inverters. By using the orientations and location data, a predefined power curve could be loaded into the inverter that then cannot be exceeded during operation. This method would primarily serve to verify the accuracy of orientation data and any discrepancies would result in energy loss. This approach is an advancement of peak clipping discussed in section 4.3, but it includes a time-dependent aspect, enabling DSOs to perform calculations using these predefined curves. Nevertheless such a solution has not been realized yet and would require inverter manufacturers to adapt to this technology and additional regulation to guarantee its functionality.

Bibliography

[1] P. Biermayr, S. Aigenbauer, C. Dißauer, M. Eberl, M. Enigl, H. Fechner, C. Fink, M. Fuhrmann, F. Hengel, M. Jaksch-Fliegenschnee, K. Leonhartsberger, D. Matschegg, S. Moidl, E. Prem, T. Riegler, S. Savic, C. Schmidl, C. Strasser, P. Wonisch, and E. Wopienka, *Innovative Energietechnologien in Österreich: Marktentwicklung 2022.* BMK, 2023.

[2] Bundeskanzleramt Österreich, *Regierungsprogramm 2020–2024.* Wien: BKA, 2020, ch. 3 Klimaschutz, Infrastruktur, Umwelt & Landwirtschaft.

[3] BMK, *Integrierter österreichischer Netzinfrastrukturplan.* Umweltbundesamt, July 2023, Draft, Last Access: 2023-10-27. [Online]. Available: https://www.bmk.gv.at/themen/energie/energieversorgung/netzinfrastrukturplan.html

[4] Bundesnetzagentur, "Marktstammdatenregister," Version 23.1.112, Last Access: 2023-05-29. [Online]. Available: https://www.marktstammdatenregister.de/MaStR/Einheit/Einheiten/OeffentlicheEinheitenuebersicht

[5] E-Control, "Anlagenregister," Last Access: 2023-10-27. [Online]. Available: https://anlagenregister.at/

[6] National Law, "Elektrizitätswirtschafts- und -organisationsgesetz," 2010, Revision dated 15.05.2023, Last Access: 2023-10-27. [Online]. Available: https://www.ris.bka.gv.at/GeltendeFassung.wxe?Abfrage=Bundesnormen&Gesetzesnummer=20007045

[7] U. Trinkner, M. Mattmann, N. Wehbring, M. Stroot, M. Meyer, and A. Ulbig, "Beurteilung des Netzanschlusses und der Netzanschlusskapazitäten in Österreich," Swiss Economics SE AG and IAEW der RWTH Aachen, Tech. Rep., June 2022, research Report.

[8] National Law, "Kapazitätsberechnungsmethoden-Verordnung – KBM-V," 2022, Published on 26.09.2022, Last Access: 2023-10-27. [Online]. Available: https://www.ris.bka.gv.at/Dokumente/BgblAuth/BGBLA_2022_II_350/BGBLA_2022_II_350.html

[9] E-Control, "Erläuterungen zur Kapazitätsberechnungsmethoden-Verordnung 2022 – KBM-V," 2022, Last Access: 2023-10-27. [Online]. Available: https://www.e-control.at/bereich-recht/verordnungen-zu-strom/-/asset_publisher/tiRyh5zzUOU7/content/kapazit%25C3%25A4tsberechnungsmethoden-verordnung-2022-kbm-v-2022-1

[10] Oesterreichs Energie, "Verfügbare Netzanschlusskapazitäten," Last Access: 2023-10-27. [Online]. Available: https://www.ebutilities.at/verfuegbare-netzanschlusskapazitaeten

[11] APCS Power Clearing and Settlement AG, "Synthetische Lastprofile," VDEW, Tech. Rep., 2023, Last Access: 2023-05-29. [Online]. Available: https://www.apcs.at/de/clearing/technisches-clearing/lastprofile

[12] E-Control, "Leitfaden für den Netzanschluss von Stromerzeugungsanlagen mit typischen Beispielen," E-Control, Tech. Rep., January 2023.

[13] National Law, "NetzdienstleistungsVO Strom," 2012, Revision dated 25.05.2023, Last Access: 2023-10-27. [Online]. Available: https://www.ris.bka.gv.at/GeltendeFassung.wxe?Abfrage=Bundesnormen&Gesetzesnummer=20008149

[14] E-Control, "TOR Teil D2: Besondere technische Regeln - Richtlinie zur Beurteilung von Netzrückwirkungen," E-Control, Tech. Rep., November 2017, Last Access: 2023-10-27. [Online]. Available: https://www.e-control.at/marktteilnehmer/strom/marktregeln/tor

[15] J. Loviscach, "Wind- und Wasserkraft: Spannungsanhebung durch Einspeisung," Online lecture video, 2014, Version 2019-04-13, Last Access: 2023-10-27. [Online]. Available: https://j3l7h2.de/videos/v.php?v=feNLW-87NLQ

[16] E-Control, "TOR Erzeuger: Anschluss und Parallelbetrieb von Stromerzeugungs- anlagen des Typs A und von Kleinsterzeugungsanlagen," E-Control, Tech. Rep., April 2022, Last Access: 2023-10-27. [Online]. Available: https://www.e-control.at/marktteilnehmer/strom/marktregeln/tor

[17] A. Monti, F. Milano, E. Bompard, and X. Guillaud, *Converter-Based Dynamics and Control of Modern Power Systems*. Academic Press, 2021, ch. 3 - Classical grid control: Frequency and voltage stability. [Online]. Available: https://doi.org/10.1016/C2018-0-02717-6

[18] E. Werderitsch and G. Kalt, "Überlegungen zur Anwendung der netzwirksamen Leistung bei Regelungen zum Netzanschluss," Presentation at IEWT 2023, TU Wien, February 2023, E-Control, Last Access: 2023-05-01. [Online]. Available: https://iewt2023.eeg.tuwien.ac.at/programme_text

[19] European Commission, Joint Research Centre, "PVGIS - Photovoltaic Geographical Information System," Last Access: 2023-08-01. [Online]. Available: https://joint-research-centre.ec.europa.eu/pvgis-online-tool_en

[20] Sandia National Laboratories, "PVLIB Toolbox for Matlab," Albuquerque. NM, USA, Last Access: 2023-10-27. [Online]. Available: https://pvpmc.sandia.gov/applications/pv_lib-toolbox/

[21] D. King, J. Kratochvil, and W. Boyson, "Measuring solar spectral and angle-of-incidence effects on photovoltaic modules and solar irradiance sensors," in *Conference Record of the Twenty Sixth IEEE Photovoltaic Specialists Conference - 1997*, 1997, pp. 1113–1116. [Online]. Available: https://www.doi.org/10.1109/PVSC.1997.654283

[22] A. Smets, K. Jäger, O. Isabella, R. van Swaaij, and M. Zeman, *Solar Energy: The physics and engineering of photovoltaic conversion, technologies and systems.* UIT Cambridge Limited, 2016, ch. 18 Location issues.

[23] Photovoltaikforum, "Photovoltaik Moduldatenbank," Last Access: 2023-05-23. [Online]. Available: https://www.photovoltaikforum.com/mdb/

[24] G. Kerber, "Aufnahmefähigkeit von Niederspannungsverteilnetzen für die Einspeisung aus Photovoltaikkleinanlagen," Ph.D. dissertation, Technische Universität München, 2011, Last Access: 2023-10-27. [Online]. Available: https://mediatum.ub.tum.de/?id=998003

[25] Fraunhofer Institut für Solare Energiesysteme, "Agri-Photovoltaik: Chance für Landwirtschaft und Energiewende," Fraunhofer ISE, Tech. Rep., April 2022, 2nd edition, Last Access: 2023-10-27. [Online]. Available: https://www.ise.fraunhofer.de/de/leitthemen/integrierte-photovoltaik/agri-photovoltaik-agri-pv.html

[26] J. S. Stein, C. Reise, J. B. Castro, G. Friesen, G. Maugeri, E. Urrejola, and S. Ranta, *Bifacial Photovoltaic Modules and Systems: Experience and Results from International Research and Pilot Applications.* International Energy Agency - Photovoltaic Power Systems Programme, 2021, ch. 3 Bifacial Modules, Last Access: 2023-10-27. [Online]. Available: https://iea-pvps.org/key-topics/bifacial-photovoltaic-modules-and-systems/

[27] J. Lopez-Garcia, "Performance testing of bifacial PV modules according to IEC TS 60904-1-2," SOPHIA reliability workshop, p. 7, May 2020, European Commission, Joint Research Centre.

[28] Meyer Burger Industries, "Dataheet - Meyer Burger Glass 370-390 Wp," Version Q1-2023-V5-UL-en.

[29] A. H. Duhis, M. Aljanabi, and M. S. S. Alkafaji, "Increasing photovoltaic system power output with white paint albedo – a scenario in Al-Mausaib City using PVSyst software," *International Journal of Power Electronics and Drive Systems (IJPEDS)*, vol. 14, no. 2, pp. 1149–1159, June 2023. [Online]. Available: http://doi.org/10.11591/ijpeds.v14.i2.pp1149-1159

[30] V. Quaschning, *Regenerative Energiesysteme: Technologie – Berechnung – Simulation*, 7th ed. Carl Hanser Verlag, 2011, ch. Sonnenstrahlung, p. 403.

[31] Siemens AG Austria, "BIFROST," Last Access: 2023-10-27. [Online]. Available: https://bifrost.siemens.com

[32] D. Hauer, F. Zeilinger, R. Mosshammer, T. Leopold, and S. Wilker, "BIFROST - A narrative simulation tool for Smart Energy scenarios - Tutorial and hands-on," in *Conference Proceedings ComForEn 2021*, Nov. 2021, Last Access: 2023-10-27. [Online]. Available: https://publik.tuwien.ac.at/files/publik_301332.pdf

[33] S. Meinecke, D. Sarajlić, S. R. Drauz, A. Klettke, L.-P. Lauven, C. Rehtanz, A. Moser, and M. Braun, "SimBench – A Benchmark Dataset of Electric Power Systems to Compare Innovative Solutions based on Power Flow Analysis," *Energies*, vol. 13, no. 12, p. 3290, Jun. 2020. [Online]. Available: https://doi.org/10.3390/en13123290

[34] Universität Kassel, Fraunhofer IEE, RWTH Aachen University, and Technische Universität Dortmund, "SimBench – Documentation," Sep. 2021, Version EN-1.0.0, Last Access: 2023-10-14. [Online]. Available: https://simbench.de/wp-content/uploads/2021/09/simbench_documentation_en_1.1.0.pdf

[35] R. Klima and S. Selberherr, *Felder: Binäres Suchen*. Vienna: Springer Vienna, 2010, pp. 174–176. [Online]. Available: https://doi.org/10.1007/978-3-7091-0393-7_13

[36] ÖVE/ÖNORM E 1100-2, "Standard voltages – Part 2: Nominal voltages for low-voltage supply systems," 2005, last Access: 2023-11-06. [Online]. Available: https://www.ris.bka.gv.at/Dokumente/Bundesnormen/NOR40164799/I_02_OEVE_OENORM_E_1100-2_2005-05-01.pdf

[37] H. Fechner, "Ermittlung des Flächenpotentials für den Photovoltaik-Ausbau in Österreich," p. 12, February 2020, Last Access: 2023-10-27. [Online]. Available: https://oesterreichsenergie.at/publikationen/ueberblick/detailseite/ermittlung-des-flaechenpotentials-fuer-den-photovoltaik-ausbau-in-oesterreich

[38] Netz Niederösterreich GmbH and Forum Versorgungssicherheit, "Stellschrauben einer sonnigen Energiezukunft," Jun. 2023, last Access: 2023-11-07. [Online]. Available: https://www.ots.at/presseaussendung/OTS_20230615_OTS0090

[39] Oesterreichs Energie, "PV-Ausbau: Positionen der E-Wirtschaft, um den zur Erreichung der Klima- und Energieziele notwendigen PV-Ausbau sicherzustellen," April 2020, Last Access: 2023-10-27. [Online]. Available: https://oesterreichsenergie.at/publikationen/ueberblick/detailseite/positionspapier-pv-ausbau